

University of Windsor
Scholarship at UWindsor

[Electronic Theses and Dissertations](#)

[Theses, Dissertations, and Major Papers](#)

1-14-2020

Automated Regulation of LiDAR Detection Range with Model-Guided Extremum Seeking Control

Youying Hua
University of Windsor

Follow this and additional works at: <https://scholar.uwindsor.ca/etd>

Recommended Citation

Hua, Youying, "Automated Regulation of LiDAR Detection Range with Model-Guided Extremum Seeking Control" (2020). *Electronic Theses and Dissertations*. 8300.
<https://scholar.uwindsor.ca/etd/8300>

This online database contains the full-text of PhD dissertations and Masters' theses of University of Windsor students from 1954 forward. These documents are made available for personal study and research purposes only, in accordance with the Canadian Copyright Act and the Creative Commons license—CC BY-NC-ND (Attribution, Non-Commercial, No Derivative Works). Under this license, works must always be attributed to the copyright holder (original author), cannot be used for any commercial purposes, and may not be altered. Any other use would require the permission of the copyright holder. Students may inquire about withdrawing their dissertation and/or thesis from this database. For additional inquiries, please contact the repository administrator via email (scholarship@uwindsor.ca) or by telephone at 519-253-3000 ext. 3208.

Automated Regulation of LiDAR Detection Range with Model-Guided Extremum Seeking Control

by

Youying Hua

A Thesis

Submitted to the Faculty of Graduate Studies
through the Department of Electrical and Computer Engineering
in Partial Fulfillment of the Requirements for
the Degree of Master of Applied Science
at the University of Windsor

Windsor, Ontario, Canada

2020

©2020 Youying Hua

Automated Regulation of LiDAR Detection Range with Model-Guided
Extremum Seeking Control

by
Youying Hua

APPROVED BY:

M.J.Ahamed

Department of Mechanical, Automotive and Materials Engineering

B.Balasingam

Department of Electrical and Computer Engineering

X.Chen, Advisor

Department of Electrical and Computer Engineering

January 14, 2020

Declaration of Co-Authorship /

Previous Publication

I. Co-Authorship

I hereby declare that this thesis incorporates material that is result of joint research, as follows:

This thesis also incorporates the outcome of a joint research undertaken in collaboration with Jie Tang under the supervision of Dr. Xiang Chen and Dr. Ying Tan. The collaboration is covered in Chapters 2, 4, and 5 of the thesis. In all cases, the key ideas, primary contributions, experimental designs and data analysis were performed by the author, and the contribution of co-authors was through the provision of the theoretical support and experimental setup.

I am aware of the University of Windsor Senate Policy on Authorship and I certify that I have properly acknowledged the contribution of other researchers to my thesis, and have obtained written permission from each of the co-authors to include the above materials in my thesis.

I certify that, with the above qualification, this thesis, and the research to which it refers, is the product of my own work.

II. Previous Publication

This thesis includes one original papers that have been previously submitted for publication in peer reviewed , as follows:

Thesis Chapter	Publication title/full citation	Publication status*
Chapter 2,4,5	Automated Regulation of LiDAR Detection Range with Model-Guided Extremum Seeking Control	submitted

I certify that I have obtained a written permission from the copyright owner(s) to include the above published material(s) in my thesis. I certify that the above material describes work completed during my registration as a graduate student at the University of Windsor.

I declare that, to the best of my knowledge, my thesis does not infringe upon anyone's copyright nor violate any proprietary rights and that any ideas, techniques, quotations, or any other material from the work of other people included in my thesis, published or otherwise, are fully acknowledged in accordance with the standard referencing practices. Furthermore, to the extent that I have included copyrighted material that surpasses the bounds of fair dealing within the meaning of the Canada Copyright Act, I certify that I have obtained a written permission from the copyright owner(s) to include such material(s) in my thesis.

I declare that this is a true copy of my thesis, including any final revisions, as approved by my thesis committee and the Graduate Studies office, and that this thesis has not been submitted for a higher degree to any other University or Institution.

Abstract

LiDAR detection is susceptible to ambient interference. Therefore, it is important to maintain LiDAR detection performance when it operates autonomously in varying environments. In this paper, an optimization approach is proposed to automatically regulate LiDAR detection range through a model-guided extremum seeking control (ESC) against the variation of ambient conditions. A neural network model is trained with experimental LiDAR data off-line to simulate the impact of ambient conditions, and an Environmental Index (EI) is proposed to classify the ambient conditions. In order to obtain the optimal LiDAR detection range for each classified ambient condition, a designed cost function is used to obtain off-line solutions for each ambient condition. In order to deal with modelling uncertainties, an on-line optimization algorithm, ESC, is employed with initial conditions originating in the results of off-line optimization. The effectiveness of this model-guided ESC mechanism is then validated with experiments involving a real LiDAR on a mobile carrier.

Keywords: autonomous operation, LiDAR, extremum seeking control

Dedication

Dedicated to God.

Acknowledgments

I would like to take this opportunity to thank my supervisor, Dr. Xiang Chen, for his elaborate guidance through my master studies . His support and feedback helped in transforming this paper into a more meaningful one. His immense passion for teaching and research have further inspired me to pursue this path in the future. I am also grateful to Dr. Ying Tan at the University of Melbourne. Thank you for the technical support in the experiments and this research.

I would like extend my gratitude to my lab colleagues, Jie Tang, Tong Zhang, Zike Lei, Fasrsam Farzadpour, and Qinyuan Tan in the Graduate Control and Robotics Lab, for their friendship, support, their constant involvement, and their valuable feedback.

I would also like to thank my committee members, Dr. Balakumar Balasingam and Dr. Jalal Ahamed, for their constructive comments, valuable feedback, positive criticism and their time in reviewing my work.

My deepest gratitude goes out to my parents. They support me both mentally and financially. Also special thanks to my friends who have been inspiring and encouraging.

Contents

Declaration of Co-authorship / Previous Publication	iii
Abstract	v
Dedication	vi
Acknowledgment	vii
List of Tables	x
List of Figures	xi
List of Abbreviations	xiv
1 Introduction	1
1.1 Introduction	1
1.2 Purpose and Objectives	2
1.3 Literature Review	3
1.3.1 LiDAR Detection Performance under Degraded Environment .	3
1.3.2 LiDAR Detection Using Learning Algorithm	5
1.3.3 ESC	5
1.4 Thesis Oultline	6
2 Preliminary	8
2.1 LiDAR Basics	8
2.1.1 LiDAR Principle	8
2.1.2 LiDAR Equation	10

2.1.3	Laser Transmitting	11
2.1.4	Neutral Density Filter	13
2.2	Neural Network	14
2.3	Environment Index	18
2.4	Perturbation-based Extremum Seeking Control	20
3	Problem Formulation	24
4	General Solution	27
4.1	Structure of Automated Regulating Mechanism	27
4.2	Optimization of Model-Guided ESC	28
4.2.1	Model-Based Off-Line Optimization Solution	28
4.2.2	A Perturbation-Based ESC	29
4.3	Detail of System Auxiliary Part	31
4.3.1	Data Processing	32
4.3.2	Switching Algorithm	32
4.3.3	PID	35
5	Experimental Validation	36
5.1	Experimental Software and Hardware Environment	36
5.1.1	Overview of Mobile-carrier Setup	36
5.1.2	Software Environments	41
5.2	Data Fitting Experiment of Model-based Off-line Optimization . . .	42
5.3	Experimental Results	49
5.3.1	Experiment I	50
5.3.2	Experiment II	56
5.4	Conclusion	59

6 Conclusion	60
6.1 Summary of Contribution	60
6.2 Future Work	61
Appendix A	62
Appendix B	63
Bibliography	64
Vita Auctoris	70

List of Tables

5.1	Parameters of fitting results of intensity vs. range	42
5.2	Analytic expressions of laser point number vs. detection range	45
5.3	Analytic expressions of laser point number vs. detection range	47
5.4	Off-line model-based optimal detection ranges \widehat{R}^*	49
5.5	Settling time (10% of final state) of model-guided ESC and traditional perturbation ESC	54
5.6	Average cost of model-guided ESC and traditional perturbation ESC in final state	54
5.7	Average laser intensity of model-guided ESC and traditional perturbation ESC in final state	55
5.8	Average laser point number of model-guided ESC and traditional perturbation ESC in final state	55
5.9	Average FOV of model-guided ESC and traditional perturbation ESC in final state	56

List of Figures

2.1	Schematic Diagram of Triangulation [1]	9
2.2	Electromagnetic wave attenuation mechanism	12
2.3	ND filters and mechanism of light transmission reduction by filters.	14
2.4	One hidden layer MLP	15
2.5	Outline of neural network for EI_n	19
2.6	Perturbation-based ESC Scheme	20
2.7	Perturbation-based ESC Structure	21
3.1	Demonstration of LiDAR detection.	25
4.1	Block diagram of model-guided ESC	28
4.2	Scheme of ESC with attenuation dither.	31
4.3	Flow chart of the algorithm.	33
5.1	Mobile-carrier used in the experiments.	37
5.2	LS02A LiDAR from LeiShen Intelligent System.	38
5.3	LiDAR covered by ND filters	39
5.4	The NVIDIA TX2	39
5.5	The Micro-controller	40
5.6	The Sketch of Omnidirection Wheel Vehicle	40
5.7	Curve fitting result of laser intensity vs. range in degraded environments	43

5.8	Experimental results and curve fitting of laser point number vs. range	46
5.9	Neural network scheme of designed experimental platform	48
5.10	Targets in Experiments I	50
5.11	LiDAR static detection results under all EIs	51
5.12	LiDAR static detection result under EI_2	52
5.13	LiDAR static detection for white paper	53
5.14	LiDAR detection results under all EIs	55
5.15	Targets in dynamic detection	57
5.16	Targets in dynamic detection	58

List of Abbreviations

EI	Environment Index
ESC	Extremum Seeking Control
FOV	Field of View
IMU	Inertial Measurement Unit
LiDAR	Light detection and ranging
MLP	Multi-Layer Perceptron
ND	Neutral Density
NN	Neutral Network
PSD	Position Sensitive Detector

Chapter 1

Introduction

1.1 Introduction

With the development of autonomous vehicles and robotics in recent years, perception of the environment is a key challenge in these fields. At the same time, LiDAR (light detection and ranging), as a mainstream environmental detection sensor, is widely used in mapping and ranging technology. However, a major problem of LiDAR is that it is vulnerable to environments[2]; therefore, perception of environment is critical and also a key challenge in many autonomous operations, such as autonomous robotic systems and vehicles, ground or aerial [3][4]. In many practical autonomous applications, the environmental conditions varies inevitably, hence, it is highly desired that an automatic regulation mechanism is developed to detect such variation and make corresponding adjustments to maintain LiDAR performance uncompromised. It is noted that, in general, adjustment of the intrinsic parameters of LiDAR is practically difficult and limited; instead, it is feasible to manipulate LiDAR detection range to improve the detection performance in a varying environment.

It must be pointed out that there exist tremendous challenges in sensing the variation of ambient conditions, due to the complexities in sources causing variation,

such as the changing weather conditions, lighting conditions, and surface reflecting conditions of targets, and lack of direct perception techniques. In this regard, LiDAR offers a valuable opportunity as it, by nature, operates in an interactive mode with the targets and the ambient environment. Although LiDAR point clouds store rich data of detection, there is a shortage of effective models of first principles for the relation between the cloud data and the ambient condition, which, in recent years, has attracted serious attention. The real challenge for the design of such a mechanism is that the models of ambient condition reported so far are not only inaccurate but also difficult to apply to develop the controller using existing design approaches.

Extremum Seeking Control (ESC) is a class of on-line data-driven optimization techniques that can find an optimal solution of dynamic or static systems without knowledge of the model [5]. It has been successfully applied to many engineering systems to generate robust optimal solutions to various optimization problems [6], [7]. As on-line optimization is usually slower than off-line optimization, in [8], a model-guided extremum seeking method was developed for the combustion phasing control problem in an automotive diesel engine. The ‘guidance’ provided by the validated engine models at operating points is shown to significantly speed up the converging process of the standard ESC algorithm in that work. This motivates the design of the closed-loop regulating control for LiDAR performance in this paper. Other techniques to improve the convergence speed while maintain the robustness of ESC such as re-tuning the amplitude of the dither signals as used in [9] are also utilized to improve the closed-loop performance.

1.2 Purpose and Objectives

The research purpose of this thesis can be posed as in a degraded environment, LiDAR automatically adjusts the detection range (R) in real time to optimize the de-

tection performance. Therefore, the objective is to present an effective control system for a mobile carrier with LiDAR to facilitate automatic detection of ambient condition change and regulation of the LiDAR detection range to maintain satisfactory LiDAR performance. For this objective, a model-aided extremum seeking controller is proposed. Moreover, a series of experiments executed to prove the effectiveness of the controller. Note that in this thesis, the impact of the environment on LiDAR focuses on the laser attenuation and not the complexity and resolution of the target. Thus, in this LiDAR system, we assume that one material surface is detected in each LiDAR scanning. This research is significant and meaningful because even though there is a great deal of literature in the area of the influence of environment on LiDAR performance, few studies mentions how to adjust LiDAR to improve detection performance. It has practical application value, and the experiments of the research prove its feasibility.

1.3 Literature Review

A large number of researchers have investigated this topic and tried to quantify the environmental impact on LiDAR.

1.3.1 LiDAR Detection Performance under Degraded Environment

Most of researchers start this topic by discussing the impact of the weather on LiDAR such as fog, rain, dust, or snow [10][11], which is more realistic and easy to verify by experimentation. Many of them have developed mathematical models for the performance degradation of LiDAR as a function of weather parameters and incorporated the models into simulations or experiments to show the impact of adverse weather on LiDAR. I call this "Weather Model Method." This method has a strong

theoretical foundation because many meteorologists have done the fundamental research. They establish the relationship between attenuation coefficient and weather parameters [12][13][14]. In rainfall case, rain rate and drop size distribution are widely used in laser transmission case, and in fog case the parameter is visibility. On this basis, many researchers tried to explore the relationship between weather parameters and LiDAR equations, or quantify the influence of degraded environment on LiDAR performance[15][16][17][18] and moreover conducted experiments to validate them, for example in literature [10][11][19][20]. However, this approach derived from the weather model will lead to model mismatches, because the weather model is very complex and is difficult to describe by several weather parameters. Most researchers can only build models on several weather parameters. Despite experimental verification, there will be model errors and model incompleteness. In this thesis, through experimentation, some off-line LiDAR detection range models under degraded environments are also obtained. However, the model-based method is only an auxiliary part of the system, used to optimize the initial state of the ESC. The model mismatch will not affect the final results.

Moreover, many other researchers have done “Experiment Method”, which focuses more on studying and analyzing the experimental results [3][21][22][23]. The literature is through doing experiments and comparing the LiDAR data by different weather parameters or even different LiDAR equipment to obtain the empirical relationship between LiDAR data and weather conditions. For example, in [21], the authors try to quantify the influence of rain on one LiDAR (Velodyne VLP-16) in different LiDAR parameters: range, intensity, and number of detected points. The results showed the intensity and the number of points decrease dramatically while the range did not change much.

1.3.2 LiDAR Detection Using Learning Algorithm

Based on machine learning technology, Robin Heinzler et al. introduced an approach to detect and classify rain or fog with LiDAR sensors only[24]. In this respect, this thesis also uses machine learning technology (neural network) to classify the environments. At the same time, in [24], a professional climate chamber is used to simulate the fog and rain cases, which is not available to most researchers.

Even though there is a great deal of literature in this area, few studies mentions how to adjust LiDAR to improve detection performance and how to develop a closed loop regulating mechanism to automatically address the performance degradation of LiDAR due to ambient condition variation. Surely, one reason is because most research tasks deal with autonomous driving and investigate the LiDAR sensor itself. Then they quantify the environmental impact and use algorithms or sensor fusion technologies to compensate for the environmental impact, which is more practical. However, in this thesis, an optimization scheme (model-guided ESC) is proposed to optimize the detection performance by adjusting the optimizer (LiDAR detection range).

1.3.3 ESC

Extremum seeking control is an old topic that was first investigated in the early 1950s. However, after a rigorous proof of the classical ESC was provided in [25], ESC generated numerous new results and applications. Various techniques have since then been developed to improve the performance of the ESC [26]. Tuning of the ESC has a great impact on its performance, a bit like a PID controller. Three parameters are usually tuned to improve the convergence: the adaptive gain, the amplitude, and oscillation frequency of the dither signal. In [27], a decaying feedback gain and a vanishing dither signal are proposed to improve the extremum seeking controller's robustness against various uncertainties. Additionally, in many ESC applications,

the ESC structure had to be carefully designed like the parameters to achieve a better optimization. In [8], a model-guided extremum seeking optimization method is applied to the combustion phasing control problem and the model guidance method is used in the cost function, which significantly improves the convergence time of the extremum seeking scheme. In this thesis, a model-guided ESC scheme is proposed with decaying dither as the excitation. Comparative experiments to show that this design is better than the classical ESC are included in the experimental part of this thesis.

1.4 Thesis Oultline

This thesis begins with a motivation and the system introduction in Chapter 1. Section 1.3 gives the relevant research directions and literature review in the fields involved in the thesis.

Chapter 2 talks about some preliminary knowledge needed in this thesis as well as newly developed Environment Index (EI). Section 2.1 introduces some LiDAR basics, which helps to understand how the environment affects LiDAR from the principle of LiDAR and laser propagation. Also, these knowledge accommodate the feature selection in the neural network model designed for EI classifying the impact of degraded environments, which introduced in Section 2.2 and Section 2.20 by introducing the basic theory of neural networks and describing the design idea of EI. Section 2.4 introduces the classical ESC. We have to know the principles of classical ESC, then we know how the system works, and the strengths of the proposed model-guided ESC.

Chapter 3 clarify the problem formulation of this research.

Chapter 4 describes the general solution of the problem: a closed-loop automated mechanism is proposed and a model-guided ESC algorithm is implemented to make sure the detection range of an LiDAR to be optimally regulated with a mobile carrier.

In particular, in Section 4.1, the structure of the closed-loop mechanism is presented while each functioning block is explained in the following sections. Section 4.2 describes the two optimization parts of this structure: Section 4.2.1 gives the details about cost functions and optimization solution of off-line model-based optimization. Section 4.2.2 is followed by the introduction of the structure and algorithm of the perturbation-based ESC with the attenuation dither.

Chapter 5 shows the experimental validation of the proposed model-guided ESC. Section 5.1 introduces the experimental software and hardware environment in this research. Section 5.2 shows the data fitting results used in the off-line model-based optimization; Section 5.3 shows the verification experiment results in different situations and the comparing results for the traditional perturbation-based ESC algorithm.

Chapter 6 ends with conclusion and future works.

Chapter 2

Preliminary

To support some technical concepts and mathematical definitions in the thesis, this chapter will give a brief introduction about LiDAR basics, extremum seeking control and neural network model.

2.1 LiDAR Basics

2.1.1 LiDAR Principle

LiDAR principally includes three parts: transmitting system, receiving system and data processing. Pulsed laser trains which are emitted from the LiDAR transmitter traverse in the air. After hitting the surface of the object, the laser reflects and scatters and part of it returns to the telescope of the receiver. According the data processing, range and light intensity data is obtained. Even more, based on an advanced reconstruction algorithm, the object's structure could be obtained.

Various ranging methods could be applied on LiDAR technology, the two main methods are time of flight and triangulation.

Time of Flight

Time of flight (ToF) is a measurement of time difference between the signal's emis-

sion and its return to the sensor which obtains the distance of the measured object. Through calculating the travel time and the speed of the signal, the distance of the object could be determined. It is noted that the signal propagation is composed of emitting and returning, so the travel time is round-trip time. Due to the measuring medium for LiDAR being light, speed of LiDAR signal is velocity of light. The range could be calculated from Equation(2.1).

$$R = \frac{c \cdot \Delta t}{2}, \quad (2.1)$$

where R - detection range(m), c - velocity of light (m/s), Δt - round-trip time (s).

Triangulation

Triangulation LiDAR generally includes a CMOS/CCD or PSD detector and a solid-state laser light source. Because based on the triangulation, the laser transmitter, laser receiver and the measured object form a triangle on a plane, shown in Figure 2.1, the distance to the object can be calculated by using geometric triangle theorem. D is the distance to be measured; F and E are the focal length of the lens and the position difference between the emitter and the lens, which are deterministic values; G is offset of the spot on the lens. With triangle similarity theory, we can get the calculation formula of the distance D [28]:

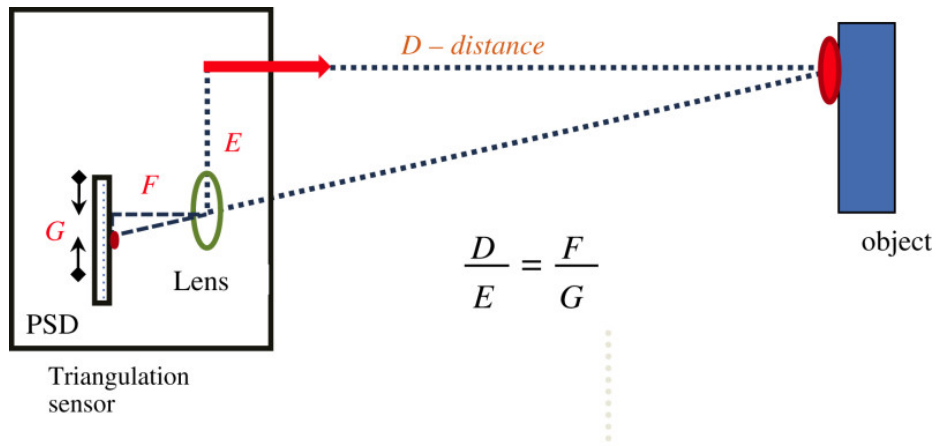


Figure 2.1: Schematic Diagram of Triangulation [1]

2.1.2 LiDAR Equation

LiDAR equation is used to compute the power returned to a receiver for given transmitted laser power, optical properties of the medium through which the lidar beam passes, and target properties. Equation(2.2) is one of the commonly used LiDAR equation [29]:

$$P(R) = P_0 G(R) \frac{A}{\pi R^2} \rho \exp \left(-2 \int_0^R \gamma(z) dz \right) \quad (2.2)$$

where $P(R)$ is the returning power received by the LiDAR from a target at distance R ; P_0 is the output power of the transmitted laser pulse; $G(R)$ represents the overlap function between the laser beam and the receiver field of view; A is the receiving aperture area; ρ is the reflectivity coefficient of the target; γ is the atmospheric attenuation coefficient, which decided by the propagation medium. And if the atmospheric attenuation does not vary significantly along the laser propagation path, Equation(2.2) can be simplified as

$$P(R) = P_0 G(R) \frac{A}{\pi R^2} \rho \exp(-2\gamma R) \quad (2.3)$$

From Equation(2.2), the reflectivity coefficient of the target and atmospheric attenuation coefficient are the most important environmental impacts on LiDAR equation. Additionally, letting the LiDAR intrinsic parameters be reduced to a single coefficient $C_s = \frac{P_0 A G(R)}{\pi}$ [10]. The LiDAR equation can be simplified as:

$$P(R) = \frac{C_s}{R^2} \rho \exp(-2\gamma R) \quad (2.4)$$

Converting Equation(2.4):

$$R^2 P(R) = C_s \rho \exp(-2\gamma R) \quad (2.5)$$

Motivated by Equation(2.5), we can guess the left side of the equation contains the information of ambient conditions, because ρ and $\exp(-2\gamma R)$ are from targets and medium of laser path. So, a new feature β can be introduced as

$$\beta \propto R^2 \cdot P(R) = C_s \rho \exp(-2\gamma R) \quad (2.6)$$

Note that $P(R)$ is normally not a measured data in LiDAR, instead, it is the laser intensity I that can be obtained from the point cloud data of LiDAR which is closely related to $P(R)$. Then the environmental impacts (target reflectivity and atmospheric attenuation $\rho \exp(-2\gamma R)$) can be characterized by the expression of the detection range and laser intensity:

$$\beta = R^2 \cdot I. \quad (2.7)$$

Apparently, β is measurable. Thus, the impact of environment factors can be approximately measured and calculated by LiDAR data. In fact, the LiDAR equation is not unique. The specific equation form and parameters depend on LiDAR specifications, like LiDAR geometry, optics properties or other mechanical structure of the LiDAR. However, the essence of LiDAR equation is still describing power attenuation from laser transmitting to receiving, and to estimate the maximum detection range and the influence factors of LiDAR system.

2.1.3 Laser Transmitting

In the LiDAR equation (2.2), $\exp\left(-2 \int_0^R \gamma(z) dz\right)$ is the attenuation term. It describes how much light is lost on the propagation way, which is from Beer-Lambert Law.

$$T = \frac{I}{I_o} = \exp(-2\gamma R), \quad (2.8)$$

where T is transmission, I is the transmitted intensity, I_0 is the incident intensity; As attenuation coefficient, γ contains two separate physical processes: absorption and scattering. So,

$$\gamma = \gamma_a + \gamma_s, \quad (2.9)$$

where γ_a and γ_s are absorption and scattering coefficients respectively. Attenuation is the energy loss of an electromagnetic wave by scattering and absorption as it traverses a particulate medium. In many other literature, attenuation is also known as extinction. Figure 2.2 shows the mechanism of electromagnetic wave attenuation.

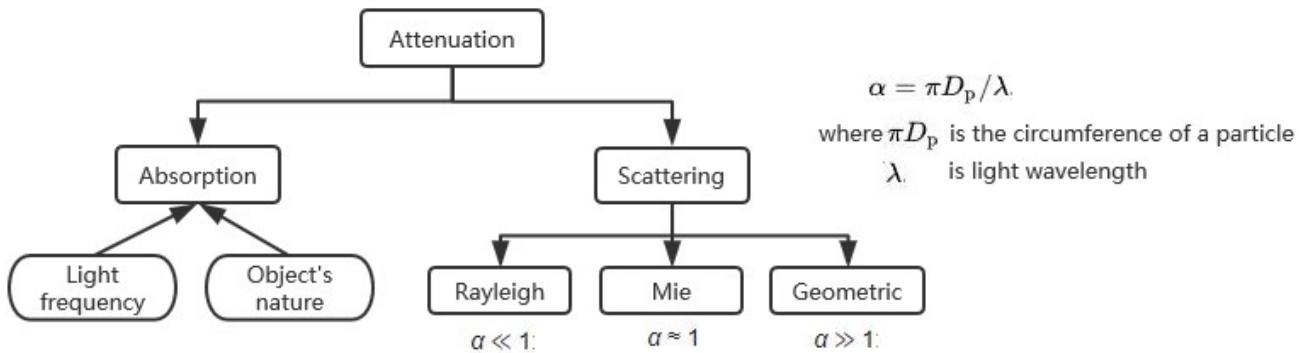


Figure 2.2: Electromagnetic wave attenuation mechanism

Absorption of light depends on the electromagnetic frequency of the light and air medium's nature of atoms, which could refer to the atmospheric window information. The atmospheric window gives the information about what portion of the electromagnetic spectrum that can be transmitted or absorbed through the atmosphere. In homogeneous media the dominant attenuation mechanism is usually absorption.[30] However, if the air is not pure, scattering will have a major impact on the attenuation of light.

Scattering of light is relatively more complicated. The degree of scattering is decided by the ratio of particle size and electromagnetic wave wavelength. For example, dry clean air, containing only a small amount of water vapor and aerosol particles,

mostly gas molecules, belongs to Rayleigh scattering because particle diameters are much smaller than the laser wavelength. In contrast for the geometric scattering, the particle size is much bigger than wavelength, like snowfall. Actually, weather and environment models are too complicated to represent by several parameters. For example, the radius of raindrop is generally considered to be 0.05mm-4mm[31], so the scattering effect of rain falls in between Mie and Geometric scattering. Rainfall is often accompanied by fog, and these two types of weather models are different. Also, in the case of snowfall, fluffy snow and small snow give rise to different models, large snowflakes will cause more complex geometric scattering. In this paper, the detail of light absorption and scattering will not be introduced.

2.1.4 Neutral Density Filter

Neutral density (ND) filters are created for an equal transmission reduction across a section of an exact spectrum. There are two types of filters: absorptive and reflective. In the experiments in this research, a group of absorptive ND filters are used. Typically, absorptive ND filters are composed of an absorbing layer or a thin metal film deposited on a glass substrate.[32] In figure 2.3, an intuitive picture of light transmission reduction by ND filters is shown. For an ND filter, the amount of optical power restricted through the filter can be determined by Optical Density (OD):

$$OD = \log_{10} \frac{I_0}{I} \quad (2.10)$$

where I_0 is the intensity of incident light and I is transmitted light. Moreover, in optics, the fraction of the optical power transmitted through the filter can be calculated as [33]:

$$T = \frac{I}{I_0} = 10^{-OD}. \quad (2.11)$$

We note that the middle part of the two equations is the same, representing the ra-

tio of incident to transmitted electromagnetic power through a material. In Equation (2.8), it actually comes from the definition of optical depth, which measures the attenuation of the transmitted radiant power in a material in natural logarithm. While Equation (2.11) expressed by optical density, which is in the form of common logarithm. To sum up, the neutral density filters can be approximately simulate the laser attenuation in propagation and implemented to realize the degraded environment. It is worth noting that this is an approximate process. Because in the propagation path of laser, which filtered by ND filters, the main attenuation is caused by filters, but not all. However, in an indoor environment, we can assume the laser attenuation caused by external conditions other than the ND filters is small.

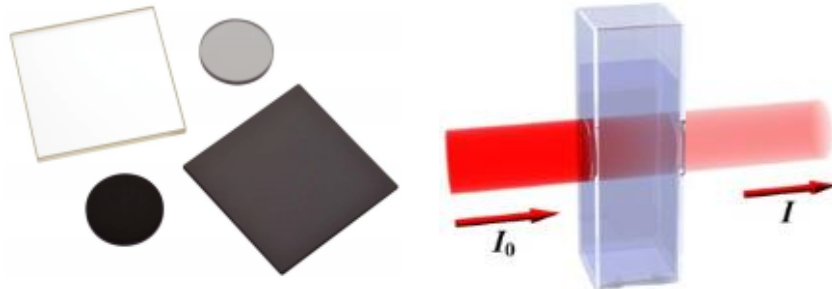


Figure 2.3: ND filters and mechanism of light transmission reduction by filters.

2.2 Neural Network

A brief introduction to the algorithm of neural networks (NN) used in the thesis is given in this section because the classification of the different ambient conditions by NN plays an important role in this model-guided ESC system. Considering that neural network is a huge and difficult field, only the techniques that will be used in this study are briefly described in this section.

Neural networks are a set of algorithms. Due to the powerful functions and model-free nature of neural networks, neural networks have developed rapidly in the past decade. A neural network is a network composed of artificial neurons or nodes, that are designed to classify and regress. One type of artificial neuron is called a perceptron, and there are some other models of artificial neurons. In this thesis, perceptron model is used as the artificial neuron model of NN, also the algorithm of this scheme is called multi-layer perceptron (MLP), which is a deep, artificial neural network composed of more than one perceptron. The MLP structure is divided into 3 parts: an input layer to receive the signal, an output layer that makes a decision or prediction, and in between those two, an arbitrary number of hidden layers that are the true computational engine of the MLP. The MLP with one hidden layer structure can approximate any continuous function [34].

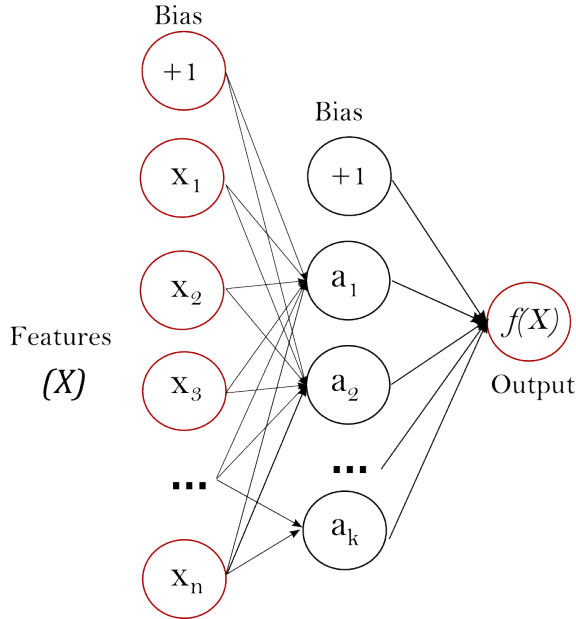


Figure 2.4: One hidden layer MLP
[35]

MLP is often applied to supervised learning problems, which learns a mapping $f(\cdot) : R^n \rightarrow R^o$ by training on a dataset of input-output pairs and gets the model relation from n-dimension input to o-dimension output. Training involves adjusting

the parameters, or the weights and biases, of the model in order to minimize error [34]. In this thesis, which means by training data labeled with environment related variables, an off-line NN model for environmental classification can be obtained. Furthermore, apply it on the model-guided ESC system based on the task. One hidden layer MLP is applied in this research and the structure of one hidden layer MLP is shown in Figure 2.4. The leftmost layer is the input layer, which represents a set of features $X = x_1, x_2, \dots, x_n$. In the hidden layer, each neuron transforms the values from the input layer with a weighted linear summation and followed by a non-linear activation function[35]. Then one neuron in the hidden layer can be derived as the follow equation [36]:

$$\mathbf{h}^{(1)} = g^{(1)}(\mathbf{W}^{(1)T}X + \mathbf{b}^{(1)}). \quad (2.12)$$

Where, $\mathbf{W}^{(1)}$ is the weights of the input layer for the neuron, $\mathbf{b}^{(1)}$ is the bias of the input layer, $g(\cdot)$ is the activation function, in this thesis, the rectified linear unit (ReLU) function is used. ReLU function is defined as the positive part of its argument:

$$g(x) = x^+ = \max(0, x), \quad (2.13)$$

where x represents the input to a neuron. In Figure 2.4, the output is a function determined by the output of the hidden layer. In order to achieve the multi-class outputs, a output vector \hat{y} should be created, and every element in the vector is $\hat{y}_i = P(y = i | X)$. Also, a softmax function is used as the output function. The softmax function is most commonly used as the output of a classifier to represent the probability distribution over multi different classes. The input of the output layer is

$$\mathbf{z} = \mathbf{W}^{(2)T}\mathbf{h}^{(1)} + \mathbf{b}^{(2)}, \quad (2.14)$$

where $z_i = \log \hat{P}(y = i | X)$. Then the format of the softmax is

$$\text{softmax}(z)_i = \frac{\exp(z_i)}{\sum_j \exp(z_j)} \quad (2.15)$$

We can see the softmax function takes as the input vector \hat{y} real numbers, and normalizes it into a probability distribution consisting of \hat{y}_i probabilities proportional to the exponentials of the input numbers. Therefore, although some vector components could be negative, or greater than one; and might not sum to 1; but after applying softmax, each component will be in the interval $(0, 1)$ and the components will add up to 1, so that they can be interpreted as probabilities and mapped the non-normalized output of a network to a probability distribution over predicted output classes [37].

Furthermore, MLP is sensitive to feature scaling. Many machine learning algorithms work better when features are on a relatively similar scale and close to normally distributed. Thus, before the MLP, scaling is often applied in case the range of value of the feature influence the classification too much. There are some feature scaling algorithms, in this research, standardization method is implemented. The form of a standardization is like

$$z = \frac{x - u}{s}. \quad (2.16)$$

where u is the mean of the training samples, and s is the standard deviation of the training samples. StandardScaler standardizes the features by subtracting the mean and then scaling to unit variance. Unit variance means dividing all the values by the standard deviation [38].

Many powerful software libraries have been designed for the development and use of neural networks. They are user-friendly designed, easy to learn and use. In this thesis, the library applied is Scikit-learn. In Section 5.1.2, a more detailed introduction of scikit-learn library will be given.

2.3 Environment Index

Environment Index (*EI*) will be introduced in this section. A basic idea of this research is to extract the information from the raw data of LiDAR, only in this way can the system achieve the automatically regulation.

Given a point cloud data matrix $X(k) \in \mathbb{R}^{n \times m}$ of LiDAR at time k ,

$$X(k)^{n \times m} = \begin{pmatrix} x_{11}(k) & x_{12}(k) & \cdots & x_{1m}(k) \\ x_{21}(k) & x_{22}(k) & \cdots & x_{2m}(k) \\ \vdots & \vdots & & \vdots \\ x_{n1}(k) & x_{n2}(k) & \cdots & x_{nm}(k) \end{pmatrix} \quad (2.17)$$

where x_{ij} represents the j^{th} feature in the i^{th} set of cloud data. An averaged feature vector $\bar{X}(k)$ can then be obtained by averaging n sets of data:

$$\bar{X}(k) = \left[\bar{x_1}(k) \quad \bar{x_2}(k) \quad \cdots \quad \bar{x_m}(k) \right]^T \quad (2.18)$$

where $\bar{x_j}(k) = \frac{1}{n} \sum_{i=1}^n x_{ij}(k), j = 1, \dots, m$.

Based on Section 2.1.2, variable β can reflect the overall impact of the environment factors LiDAR according to Equation(2.6) and (2.7); in addition, the laser intensity I is an environment-related parameter and detection range R is the optimizer of the system. Therefore, a feature vector is selected as

$$\bar{X}(k) = \left[R(k) \quad I(k) \quad \beta(k) \right] \quad (2.19)$$

to characterize the environmental-related features of the LiDAR data. Because there is no effective model of first principles to characterize the relation between the feature vector, which essentially is derived from the point cloud data of LiDAR, and the environment factors, therefore a data-induced approach is adopted to model this

relation. In this thesis, a neural network model is applied to train the feature vector in Equation (2.19) and make a prediction on the ambient conditions.

In particular, a new index called Environment Index EI is proposed to classify the impact of environment factors as driven by the feature vector $\bar{X}(k)$ which can be calculated from a trained neural network model based on feature vector (2.19). In this thesis, a four-class classification is designed according to the experimental conditions, which detailed in Chapter 5 and restrictions on environmental knowledge. The basic idea of EI is an environmental reference or an index, which does not have a clear physical meaning. It divide the whole ambient condition into several degrees, EI give a reference to systems or sensors: what kind of ambient condition they are in. Systems and sensors operate and optimize based on it. The classification of this research is shown in Figure 2.5, although a finer classification is possible in practice as needed.

$$EI_n = n, n = 1, 2, 3, 4 \quad (2.20)$$

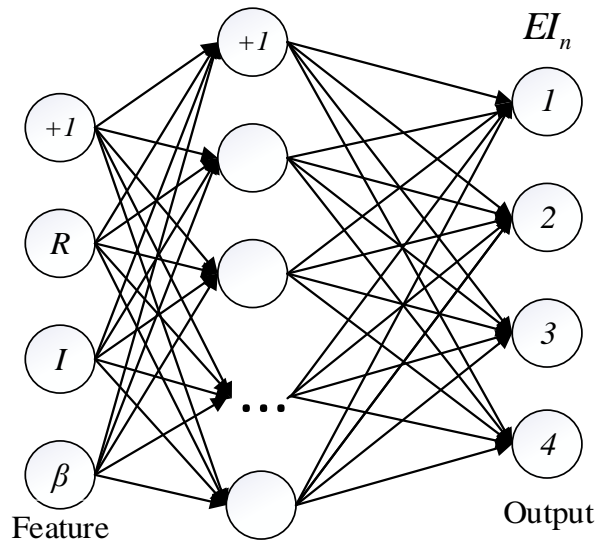


Figure 2.5: Outline of neural network for EI_n

2.4 Perturbation-based Extremum Seeking Control

As the main optimization unit of the model-guided ESC system, a simple principle and introduction of the perturbation-based ESC will be introduced in this section.

ESC is a branch of adaptive control, which invented in 1922. It is an online model-free method in which people do not need to know the system model, but only the output measurements. The basic idea behind the scheme is to perturb the direction of gradient of the system with a slow periodic signal which shown in Figure 2.6. It mainly focuses on the gradient of the performance function or cost function, which can be regarded as a steady-state map from the optimizer to the performance of cost of the system. The gradient will be zero when the output reaches the extremum value.

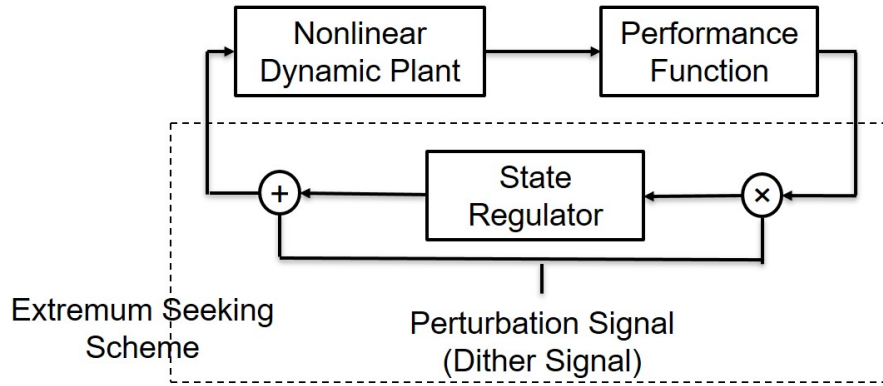


Figure 2.6: Perturbation-based ESC Scheme

There are many versions of extremum seeking. In this thesis, a classical perturbation-based ESC is focused. As the most common version, the perturbation signals with sinusoid function is mostly used. The purpose of the perturbation is estimating the gradient of the unknown cost function that is being optimized. The simplest classical perturbation-based ESC scheme is shown in Figure 2.7. $J(\theta)$ is the cost function, also is the output and θ is the input.

In Figure 2.7, $\hat{\theta}(t)$ is the real-time estimated optimal point, $\theta(t)$ is the actual

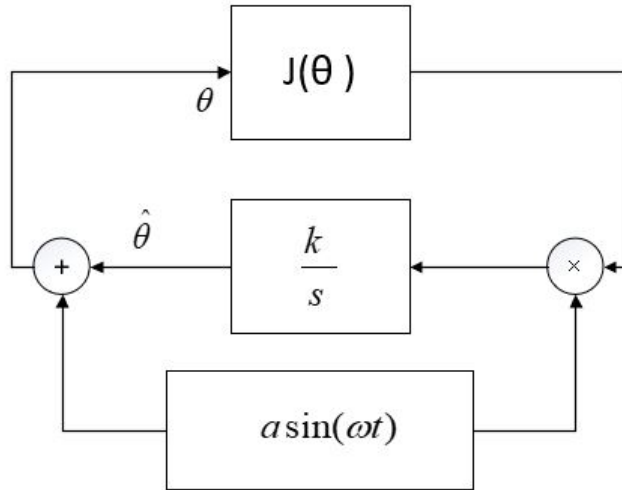


Figure 2.7: Perturbation-based ESC Structure

input and here we assume the unknown optimal value of $J(\theta)$ is θ^* . In the system, we do not need to know the analytic expression of $J(\theta)$, however, $J(\theta)$ should be measured. At the same time, we should know the sign of $J''(\theta)$, namely, the system has a maximum or a minimum, and then the sign of adaption gain k should satisfy as $sgn k = -sgn J''(\theta)$.

Actually, input $\theta(t)$ is based on $\hat{\theta}(t)$ but is perturbed by the signal $a \sin(\omega t)$ for the purpose of estimating the unknown gradient of $J(\theta)$. Then we have the following relationships:

$$\theta = \hat{\theta} + a \sin(\omega t) \quad (2.21)$$

At the same time, we define the error between the estimate $\hat{\theta}$ and the unknown optimal value θ^* is

$$\tilde{\theta} = \hat{\theta} - \theta^*. \quad (2.22)$$

The key of the ESC is to prove that $\tilde{\theta}$ can converge towards zero, which means as time goes by, the system will continue to approach the optimal solution. The following is the proof process for stability of the ESC with a static single-input system. The proof process references [39] and [40].

If we do the second-order Taylor expansion of $J(\theta)$ near θ^* and drop the higher order elements, we have

$$J(\theta) \approx J(\theta^*) + \frac{J''(\theta^*)}{2} (\theta - \theta^*)^2, \quad (2.23)$$

where $J''(\theta)$ is the second-order derivative of $J(\theta)$. Based on Figure 2.7, the estimated value is governed by the differential equation

$$\dot{\hat{\theta}} = k \sin(\omega t) \cdot J(\theta). \quad (2.24)$$

Substituting Equation (2.23) into Equation (2.24) and Equation (2.21) into Equation (2.22), we can get

$$\begin{aligned} \frac{d\tilde{\theta}}{dt} &\approx ka \sin(\omega t) \left[J(\theta^*) + \frac{J''(\theta^*)}{2} (\theta - \theta^*)^2 \right] \\ &= ka \sin(\omega t) \left[J(\theta^*) + \frac{J''(\theta^*)}{2} (\tilde{\theta} + a \sin(\omega t))^2 \right] \end{aligned} \quad (2.25)$$

Expanding the right-hand side, one obtains

$$\begin{aligned} \frac{d\tilde{\theta}}{dt} &\approx ka \sin(\omega t) J(\theta^*) + ka^3 \frac{l''(\theta^*)}{2} \sin^3(\omega t) + ka \frac{J''(\theta^*)}{2} \sin(\omega t) \tilde{\theta}(t)^2 + ka^2 J''(\theta^*) \sin^2(\omega t) \tilde{\theta}(t) \end{aligned} \quad (2.26)$$

In Figure 2.7, the integrator k/s with the adaption gain k is an averaging algorithm. A theoretically rigorous time-averaging procedure allows to replace the above sinusoidal signals by their means, thus the first three terms equal to zero. Then Equation (2.25) becomes

$$\frac{d\tilde{\theta}}{dt} = \frac{ka^2 J''(\theta^*)}{2} \tilde{\theta}(t), \quad (2.27)$$

which can be rewritten as

$$\frac{d\tilde{\theta}}{\tilde{\theta}} = \frac{ka^2 J''(\theta^*)}{2} dt. \quad (2.28)$$

Integrating two sides of Equation (2.28):

$$\ln \tilde{\theta} - \ln \tilde{\theta}_0 = \frac{ka^2 J''(\theta^*)}{2}(t - t_0). \quad (2.29)$$

where t_0 is the initial time and $\tilde{\theta}_0$ is the initial input error. Finally, we can get

$$\tilde{\theta} \approx e^{\frac{ka^2 J''(\theta^*)}{2}(t - t_0) + \ln \tilde{\theta}_0}. \quad (2.30)$$

According to the assumption about the signs of k and $J''(\theta)$:

$$k \cdot J''(\theta) < 0, \quad (2.31)$$

which means

$$\frac{ka^2 J''(\theta^*)}{2} < 0. \quad (2.32)$$

From the equations above, it follows that

$$\lim_{t \rightarrow \infty} \tilde{\theta}(t) \approx \lim_{t \rightarrow \infty} e^{\frac{ka^2 J''(\theta^*)}{2}(t - t_0) + \ln \tilde{\theta}_0} = 0, \quad (2.33)$$

which implies the input will approach the optimal value when time goes by. However, this analysis about the optimum is valid only for static system and locally. The cost function of the ESC system in this thesis is a static single-input map of the quadratic form. Meanwhile, based on model-guided way, local condition of the ESC can be achieved. Therefore, the stability of the ESC system in the thesis is proved.

For the non-local conditions, [41] shows under appropriate conditions, if the parameters in the controller are appropriately adjusted, the non-local stability result is proved.

Chapter 3

Problem Formulation

The problem formulation of this research will be clarified in this chapter. In order to satisfy the LiDAR detection performance in varying environments, a cost function for optimization is proposed. Based on the characteristics of the LiDAR used in this study and the meaningful detection performances, laser intensity I , laser return point number PN , and field of view FOV are chosen as the targeted performances. Thus the following cost function should like

$$J(R) = J(I(R), PN(R), FOV(R)) \quad (3.1)$$

Laser intensity indicates the quality of return laser signal. A large value of laser intensity represents the echo effect of the laser signal is good and the detection has a high confidence. However, inverse relationship between laser intensity and detection range means the largest laser intensity is at the minimum detection range, which is meaningless in actual application. Hence we assigned a fixed value I^* for I as required by customized specification. Laser return point number indicates the effective detection area of the LiDAR. PN^* is the optimal value of PN . In this study, $PN^* = \max(PN)$, because it is expected all laser point should be returned in the optimal case. At the same time, we hope that FOV is as large as possible to enhance

the LiDAR efficiency. Figure 3.1 demonstrates a picture of LiDAR detection.

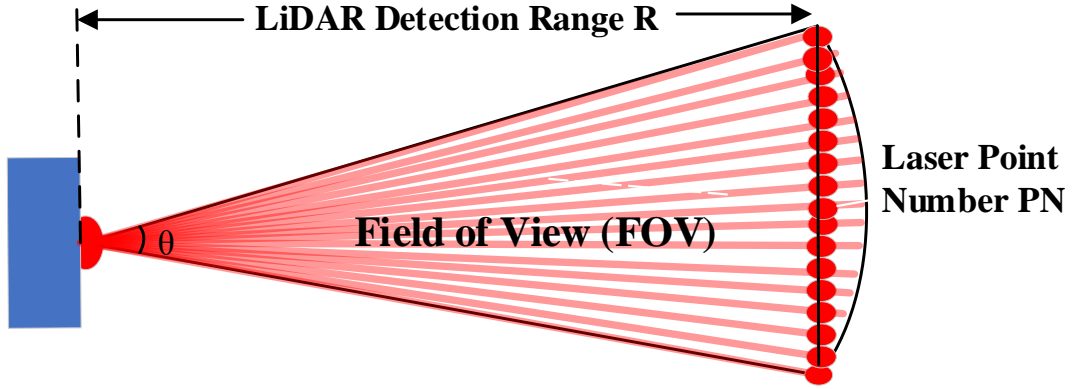


Figure 3.1: Demonstration of LiDAR detection.

According to above, the cost function is characterized in Equation (3.2) as

$$\begin{aligned} J(R) = & \alpha_1 \cdot \eta_1 \cdot (I(R) - I^*)^2 + \alpha_2 \cdot \eta_2 \cdot (PN(R) - PN^*)^2 \\ & - (1 - \alpha_1 - \alpha_2) \cdot \eta_3 \cdot FOV(R) \end{aligned} \quad (3.2)$$

where α_1 and α_2 are weighting factors determined by the relative significance among three performance variables, and η_1 , η_2 , η_3 are elastic constants that are used to normalize the variables of $J(R)$ in a comparable range. As stated in Section 2.20, the EI_n is proposed to classify the impact of environments. Correspondingly, the models of $I(R, EI_n)$, $PN(R, EI_n)$, and $FOV(R, EI_n)$ can be obtained through nonlinear fitting of the experimental data for each EI_n as it is practically difficult to derive physical models in the first principle, the details of which will be presented in Section 5.2. Thus, a set of cost functions $J(R, EI_n)$ can be employed according to the value of EI_n . Note that I and PN are in opposite trend with respect to FOV as functions of R in the reality of LiDAR; the cost function is, hence, concave within a range of $[R_{min}, R_{max}]$, and the optimal detection range corresponding to EI_n can be obtained

by solving the optimization problem in Equation (3.3):

$$J\left(\widehat{R}^*, EI_n\right) = \min_{R \in [\min, R_{\max}]} J(R, EI_n). \quad (3.3)$$

Meanwhile, according to the classification of EI in (2.20), optimal detection ranges based on EI can be obtained:

$$\widehat{R}^* = \langle \widehat{R}_1^* \widehat{R}_2^* \widehat{R}_3^* \widehat{R}_4^* \rangle. \quad (3.4)$$

Therefore, a fast selection of the detection range can be off-line optimized by looking up the value of EI_n . However, this model-based off-line method is not accurate at all as there exist errors in the data-induced models of $I(R, EI_n)$, $PN(R, EI_n)$, and $FOV(R, EI_n)$. Thus, the ESC algorithm is naturally considered and implemented to find the real optimal R^* in each classified impact range of environment as indicated by EI_n .

The arguments in the ESC are set as same as the targeted performances, also the cost function of the ESC is consistent with the previous method, which means Equation (3.2) works on the ESC. However, compared to the previous method, the model-based $I(R)$, $PN(R)$, and $FOV(R)$ become real-time measured values, not determined by the experimentally fitted data.

Note that, while the model-free nature of the ESC algorithm can find the optimal detection range based only on the point cloud data of LiDAR, regardless of the modelling knowledge of the LiDAR performance vs. the environment, the convergence process of the ESC algorithm is generally slow and not effective. Therefore, a model-guided ESC approach is proposed in this paper to combine the off-line optimized detection range \widehat{R}^* as the estimation of R^* and the on-line ESC algorithm to achieve both the convergence efficiency and the robustness in order to find the real optimal detection range R^* . The solution of this approach is presented in the next section.

Chapter 4

General Solution

In this chapter, a closed-loop automated mechanism is proposed and a model-guided ESC algorithm is implemented to solve the main research problem raised in this thesis that maintain the LiDAR detection performance in different environments by regulating the detection range. Furthermore, a mobile carrier mounted a LiDAR is conducted to optimally regulate the detection range to verify the proposed structure. In particular, in Section 4.1, the structure of the closed-loop mechanism is presented while each functioning block is explained in Section 4.2.1 and 4.2.2.

4.1 Structure of Automated Regulating Mechanism

Based on the problem formulation and the preliminary knowledge of physically realization and classification of the degraded environments, a general solution is proposed – a modal-guided ESC. The closed-loop automated regulating mechanism is shown in Figure 4.1. While EI_n can be obtained on-line from the trained neural network model, the switching algorithm is to determine if the ambient environment is changed significantly or not based on the value of EI_n , hence, determines if the estimated optimal LiDAR detection range \widehat{R}^* corresponding to EI_n should be applied to reset the ESC algorithm or not. If no significant change of environment is detected,

the ESC algorithm will continue to search the real optimal detection range R^* without interruption based on (I, PN, FOV) derived from the point cloud data. At the same time, a dither amplitude reset algorithm in ESC helps the ESC convergent fast when the system optimized by ESC. Finally, R^* is applied as the reference signal R_{ref} of the PID controller to regulate the movement of the mobile carrier to drive LiDAR to the desired detection range.

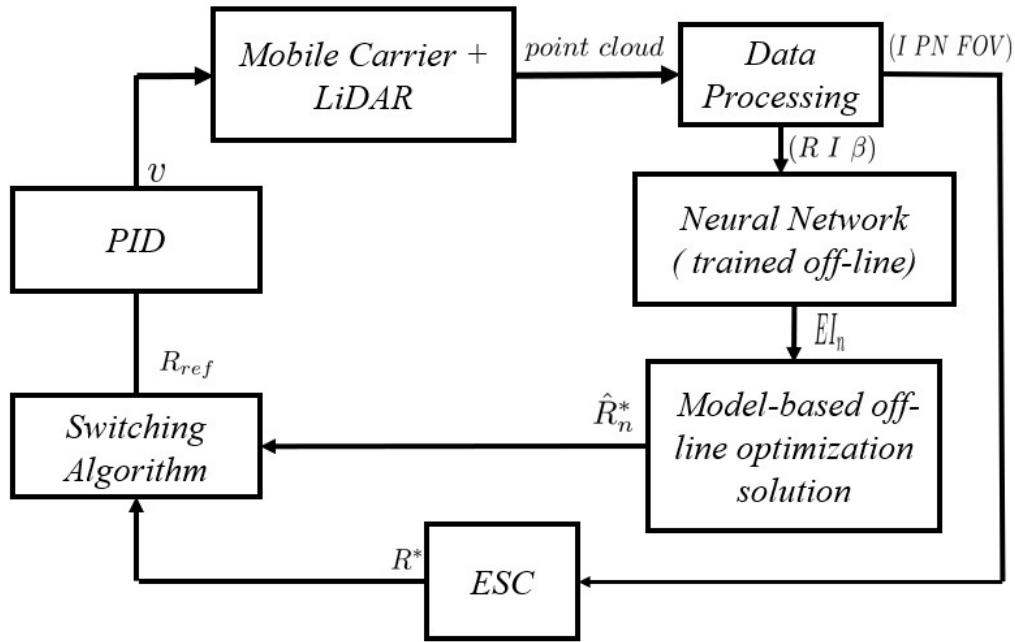


Figure 4.1: Block diagram of model-guided ESC

4.2 Optimization of Model-Guided ESC

4.2.1 Model-Based Off-Line Optimization Solution

Before getting the model-based optimization solution, EI should be predicted. As stated in Section 2.2 and 2.20, the parameters and detail of the NN model for EI_n classification is written in Appendix B. The model-based off-line optimization solution is based on the cost function (3.3), and the corresponding models of $I(R, EI_n)$, $PN(R, EI_n)$, and $FOV(R, EI_n)$ should be derived to find the values of \widehat{R}^* . Since the

physical models do not exist, in this study, the analytic expressions of $I(R, EI_n)$ and $PN(R, EI_n)$ are obtained through non-linear fitting of experimental data. Also, the analytic expression of FOV can be derived from R and PN , because the FOV in this thesis represents the detecting area of LiDAR, which can refer to Figure 3.1. The FOV will be approximated to be a sectorial area to simplify the computing, as:

$$FOV = \pi R^2 \times PN/360. \quad (4.1)$$

Note that PN actually indicates the value of the angle θ as the LiDAR used in our study provides a resolution of $1^\circ/\text{laser point}$. Meanwhile, α_1 , α_2 , α_3 , η_1 and η_3 should be carefully selected, because they did not only decide the weights for the three targeted performances but also to make the cost function $J(R)$ concave in order to ensure the \widehat{R}^* is unique.

4.2.2 A Perturbation-Based ESC

A standard perturbation-based ESC, which has been widely used in many applications due to its simplicity, is used in this project. A transitional perturbation-based ESC is introduced in Section 2.4. In this thesis, the structure is shown in Figure 4.2, and it can be seen the algorithm of the dither is improved. In traditional ESC, the cost to be optimized is denoted as J , which multiplies a dither signal $a\sin(t)$ and passes through an Integration with a positive gain k . As indicated in Corollary 1 in [41], if there is a local unique optimal value, the ESC diagram will drive the output of ESC to a small neighborhood of this local optimum. Usually the amplitude of the dither needs to be small in order to obtain a larger domain attraction and a smaller ultimate bound at the cost of slow convergence speed. In order to speed up the convergence speed, a larger “ a ” is needed, resulting in fast convergence and a large variation around the optimum [9]. To balance the convergence speed and optimal performance

(the ultimate bound), a decaying dither amplitude $a(t) = a_0 \cdot e^{-\lambda t}$; $a(t) \geq a_{min}$ is applied to the system. Then, in a stable environment, a decaying dither applied to decrease the “ a ” to obtain a smaller ultimate bound, which means a more precise position of convergence and smaller variation in optima. On the contrary, if the LiDAR encounters a large environmental disturbance, the operating point of the target detection performance changes, and the ESC needs to search the extremum value again to optimize, a fast convergence is expected. Therefore, a dither amplitude reset algorithm is applied in this improved algorithm. We set $a_0 = 0.2$; $\lambda = 0.07$; $a_{min} = 0.01$, where the value of a_{min} is to keep some robustness with respect to noises. Meanwhile, it is noted that because the ESC use the same cost function (3.3) with the model-based method, in last section 4.2.1, a concave cost function is ensured in every EI. Thus, a local unique optimal condition in [41] is set.

With the consideration of switching in different operating point, the idea of the algorithm of resetting condition for the dither amplitude is as follows. That is two thresholds J_{abn} and J_{stab} are used to represent abnormal cost and normal cost. It is noted that the perturbation-based ESC is a local optimal algorithm with an unknown domain of attraction. Hence some estimation upper bound of the domain of attraction J_{abn} from experience is used. If the measured cost value $J > J_{abn}$ consecutively, which means that the system is outside the domain of attraction, the algorithm resets the dither amplitude in order to restart the algorithm. Similarly, when the cost value $J < J_{stab}$ consecutively, the dither starts decaying and variation decrease.

In the context of this work, there is an unknown nonlinear mapping Q between the cost function (3.1) and the control input R such that

$$J(R) = J(I(R), PN(R), FOV(R)) = Q(R). \quad (4.2)$$

The control objective is to find an optimal solution R^* such that the cost is minimized,

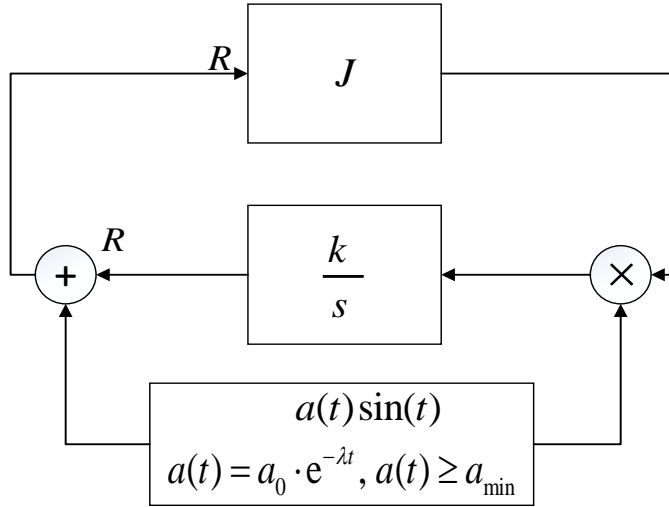


Figure 4.2: Scheme of ESC with attenuation dither.

$$Q(R^*) = \min_{R \in [R_{min}, R_{max}]} Q(R) \quad (4.3)$$

where R_{min} and R_{max} are minimum and maximum detection range of the LiDAR. The knowledge of the upper and lower bound is used to modify ESC with the standard projection method to ensure that the updating of R is within these bounds. As ESC is model free, the analytical expression of $I(R)$, $PN(R)$ and $FOV(R)$ is not needed. Also, these three arguments and the detection range can easily get from the LiDAR, so the cost and input can be measured.

4.3 Detail of System Auxiliary Part

In this section details of each block in block diagram 4.1 are illustrated, in order to clearly and thoroughly describe the entire model-guided ESC system.

4.3.1 Data Processing

Data processing is a basic part of the system. Its function is to obtain the data we need through various calculations and transformations of the LiDAR raw data or the inherent parameters of the system. As can be seen from the figure 4.1, the data processing mainly includes two parts: one is to obtain the features ($R \ I \ \beta$) of the neural network from the LiDAR real-time detection performance and use them to evaluate EI ; the other is to obtain the three arguments for ESC calculation.

Among them, detection range R and laser intensity I are directly from LiDAR point cloud, and the rest need further calculation based on point colud. In every scanning of LiDAR, PN can be obtained by counting the number of Lidar points with effective feedback, which means the returning point has R and I values within the specified range. Meanwhile, from Equation (2.7) and Equation (4.1), β and FOV can easily calculated from point cloud and PN .

4.3.2 Switching Algorithm

Switching algorithm plays an important role in the entire system. It's up to it to decide which optimization method orient the system. The optimal detection range from the model-based way is \widehat{R}^* , which value decided by cost function (3.3) according to EI_n . On the other hand, from the ESC is R^* . So, choose one from the above two optimization solution, the switching algorithm output R_{ref} as the actual optimization instruction to control the movement of the mobile-carrier. The switching algorithm has different judgment criteria in three different situations. They are the initial state, running state and protection state of the system.

a) Initial State: Every time the system is started, the switching algorithm selects the model-based optimization unconditionally, in order to enable the ESC to start at an optimal initial point. Then the system switches to the ESC algorithm according to the error between the measured detection range and the optimized value from

model-based solution. A threshold δ_0 is set; when the error is smaller than δ_0 , the system thinks that the car has reached the optimization point, it will switch to ESC; and the ESC takes over the following optimization task.

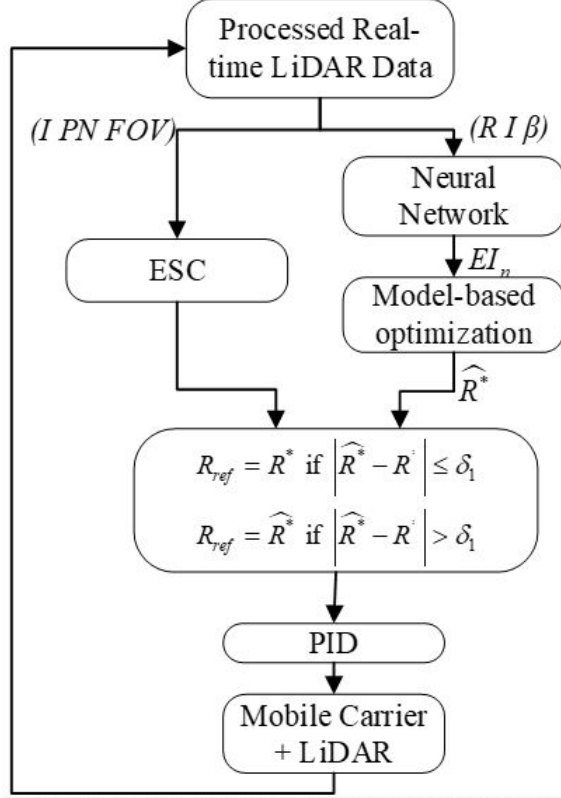


Figure 4.3: Flow chart of the algorithm.

b) Running State: When the system is formally controlled by ESC, the control mode of the system will be slightly more complicated. Because the ESC has an internal dither amplitude reset algorithm. When the disturbance of the system is small, the ESC's dither amplitude reset algorithm can accelerate the convergence of the ESC; but when the disturbance of the system is large, if the distance is completely optimized by the ESC, the convergent speed will be too slow, even if the ESC amplitude is large enough. In this case, the system is optimized by the model-based way in order to faster optimization to the optimal detection range. Therefore, the judgment criteria is set as when the error between the measured detection range and

the optimized value from model-based solution. Another threshold δ_1 is set; when the error is larger than δ_0 , the system judges that the system error is too large and the model-based optimization takes over the optimization task to get a fast control mode. The flow chart 4.3 shows the identification process of the system in the running state.

c) Protection State: In order to protect the operation security of the mobile carrier, a protection program must be added during the system operation. This program is included into the switching algorithm. Although in the specification of the experimental LiDAR the nominal maximum detection range is 4m, in actual case, it can reach 5m. Because the operation of the system is based on the point cloud data of the LiDAR, once the LiDAR has no effective returning data, the entire system will crash. So a value slightly less than 5m is set as the maximum detection range, this maximum detection range R_{max} is 4.7m. Similarly, a minimum detection range R_{min} is set as 0.5m.

The following is the pseudo code of the switching algorithm:

Algorithm 1 Switching Algorithm

Input: R^* , \widehat{R}^* **Output:** R_{ref}

```

1: System start-up
2: while  $R \in [R_{min}, R_{max}]$  do
3:   Model-based off-line solution:  $R_{ref} \leftarrow \widehat{R}^*$ 
4:   if  $|\widehat{R}^* - R| \leq \delta_0$  then
5:     ESC:  $R_{ref} \leftarrow R^*$ 
6:   else
7:     model-based off-line solution:  $R_{ref} \leftarrow \widehat{R}^*$ 
8:   end if
9:   if  $|\widehat{R}^* - R| \leq \delta_1$  then
10:    ESC:  $R_{ref} \leftarrow R^*$ 
11:   else
12:     model-based off-line solution:  $R_{ref} \leftarrow \widehat{R}^*$ 
13:   end if
14: end while

```

[1]

4.3.3 PID

The kinematics of the mobile-carrier is four omnidirectional wheel, also based on the mechanical structure of the mobile-carrier, the mobile-carrier is controlled by the velocities of the four wheels. From the optimal detection range to the velocity of the wheel, a PID controller is used here to regulate the velocity of the wheel by the real and optimal detection ranges. Specifically in this thesis, because there are many kinds of running states in the controller, PID parameters corresponding to each running state are also different.

Chapter 5

Experimental Validation

This section presents the experiments that are designed to validate the proposed regulating mechanism.

5.1 Experimental Software and Hardware Environment

5.1.1 Overview of Mobile-carrier Setup

The hardware platform of the mobile-carrier consists of the following four parts: a LiDAR, a high-level master controller, a low-level micro-controller and kinematic parts of the mobile-carrier. The low-level controller is a customized board based on STM32f103RCT6, which is used to drive the motors according to the linear and angular velocities sent from high-level controller. The NVIDIA TX2 developer board is used as the high-level master controller. All computing power consuming programs are calculated on TX2, like optimization results, switching algorithm of off-line optimization and ESC, data recording and so on. The NVIDIA TX2 controls the mobile-carrier just by sending linear and angular velocity to the low-level controller. Meanwhile, the peripheral sensors are connected to the TX2, including a LiDAR and

an IMU. The laptop is used to control the mobile-carrier start/stop.

A picture of the omnidirectional vehicles used in this thesis shown in Figure 5.1. Each side of the vehicle is 260mm, the height of the vehicle is 275mm, and the motor drives and controller are placed in the space between the platform and ground. With the selected motor and arrangement mechanism, the vehicles have maximum linear and angular velocity 1.2 m/s and 5.3 rad/s respectively. Special thanks for my colleague Jie Tang, the basic kinematics of the mobile-carrier is based on his design and build. Also, many contents of this section Section5.1.1 references his master thesis [42].

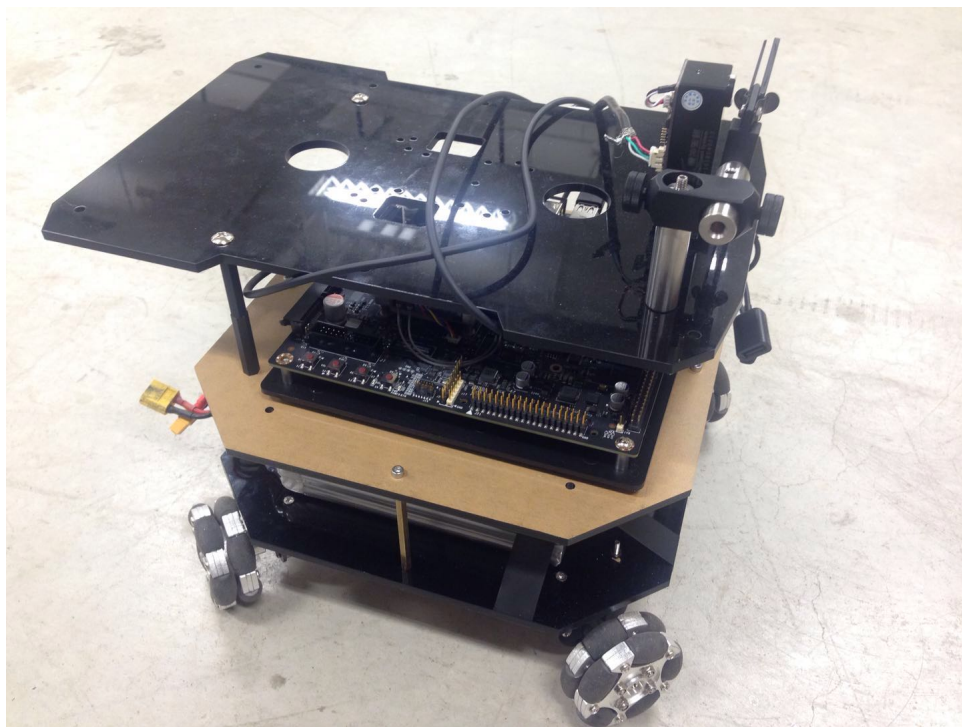


Figure 5.1: Mobile-carrier used in the experiments.

LiDAR

A solid state LiDAR LS02A used in the experiments, which manufactured by LeiShen Intelligent System Company. The specification of LS02A is shown in Appendix A. LS02A is a low-cost, lightweight LiDAR, and supports Linux and Windows systems, which applicable to a wide range of systems. Under Linux system, it can implemented

on ROS (Robot Operating System), then it is convenient to communicate with the host and other auxiliary equipments. Considering its lightweight and solid-state characteristics, it is easy to install on the mobile-carrier, and has long service life and high stability.



Figure 5.2: LS02A LiDAR from LeiShen Intelligent System.

In the experiments, three ND filters with OD=0.2, 0.6, and 1.3 are used in combination, which purchased from Thorlabs, Inc. Total of 7 combinations can be generated for OD=0 (no filter used), 0.2, 0.6, 0.8, 1.3, 1.5, 1.9. From Equation (2.11), OD value can be converted to the transmittance in percentage, that is, 100%, 63%, 25%, 16%, 5%, 3% and 1.25%, which simulates the varying ambient conditions. In the experiment, ND filters are mounted in front of the scanner of LS02A, but not cover the receiver like in Figure 5.3. Then, the emitted laser from the LiDAR is attenuated by an approximate quantization.

High-level master controller –NVIDIA TX2

The master controller is responsible for those computation consuming calculations, which may include processing sensor information, proposed algorithm calculation and network connection. Here the NVIDIA TX2 are used in the project which is a power-

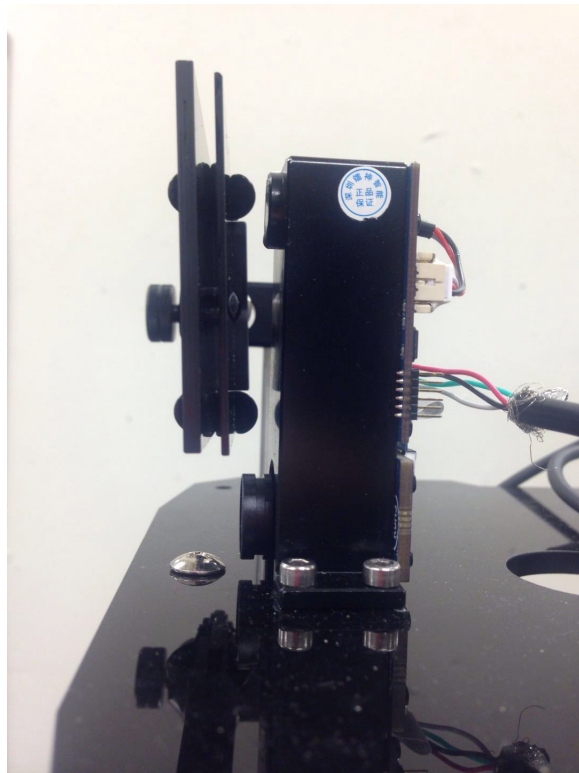


Figure 5.3: LiDAR covered by ND filters

efficient high performance embedded device with GPU inside.



Figure 5.4: The NVIDIA TX2

Low-level Microcontroller

The low-level controller used in the project is a STM32 based customized controller, which embedded the TB6612FNG motor drive chip, power module and USB series convert chip. The microcontroller board response for resolving the control command and converting to the speed on each motor, meanwhile, calculate the real

velocity based on the encoder signal.



Figure 5.5: The Micro-controller

Kinematic parts of the mobile-carrier

There are several of different kinematic models for vehicles, such as, differential two wheels, omnidirectional, ackerman, mecanum, etc. In this experiment, an omnidirectional wheel mobile carrier is used to test the algorithm. A general sketch of the omnidirectional wheel vehicle is shown in Figure 5.6. With the $\phi = 45^\circ$ in Figure 5.6, the wheels are orthogonal. For the velocity control of chassis, four PID controllers are used to track the desired linear and angular velocities by controlling four motor drives.

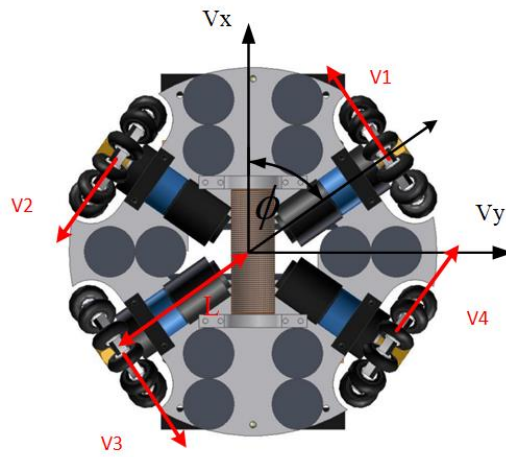


Figure 5.6: The Sketch of Omnidirection Wheel Vehicle

5.1.2 Software Environments

ROS

ROS is the abbreviation of **R**obot **O**perating **S**ystem and ROS is a distributed framework for developing and testing robotics software or algorithms [43], which supports two mainstream language python and C++. Because it has a healthy-developed developer community, many robot and peripheral device developer works on it and post much many device drivers and applications based on ROS. At the same time, it provides bunch of services, including hardware abstraction, low-level device control, implementation of commonly-used functionality, message-passing between processes, and package management. ROS has a distributed developing and running structure. By Using the publish-subscribe mechanism, each node (program or process) can subscribe to so-called topics and push message to others and in this way, the interaction among devices and algorithms. ROS also provide the data recording package named rosbag. By using rosbag, it is easy to record different types message data for late analyzing like, LiDAR data and odometer [42].

Scikit-learn

Scikit-learn is a free software machine learning library for the Python programming language, at the same time, it is designed to interoperate with the Python numerical and scientific libraries NumPy and Scipy [44]. Many application program interfaces (APIs) based on different learning algorithms are well-designed in scikit-learn library, so customized effects can be achieved and compared by adjusting the different learning algorithms or the different parameters of them. Meanwhile, by the API, the training models are easily exported and implemented off-line. In the thesis, the neural network models (supervised) are used. Because scikit-learn is for Python programming language, the neural network algorithm can easily be written as a node in ROS, plays its role and combines with other programs.

5.2 Data Fitting Experiment of Model-based Off-line Optimization

In order to validate the methodology in Section 4.2.1, the experiments are conducted to obtain the empirical relation between the targeted performances: laser intensity I , laser point number PN , field of view FOV versus detection range in order to calculate \widehat{R}^* . Move the LiDAR from $0.5m$ to the maximum range, where no LiDAR data returns, and record the data. We can get the nonlinear fitting analytical expressions about I , PN , and FOV with respect to range. After that, a set of cost function (3.3) and the corresponding \widehat{R}^* in (3.4) obtained, the values of which is the model-based off-line optimization solution in the diagram 4.1.

Laser intensity vs. detection range

As for laser intensity, by multiple comparisons, general model Power2 in MATLAB curve fitting tool (cftool) is the best fit. The fitted curves are shown in Figure 5.7. From Figure 5.7, the relationship of laser intensity and detection range in degraded environments performs well in the form of $f(x) = a \times x^b + c$ with different parameters. Table 5.1 shows the results of the parameters of fitting results from MATLAB.

Table 5.1: Parameters of fitting results of intensity vs. range

OD	a	b	c
0	1017	-1.331	332.9
0.2	805	-1.608	363
0.6	633.8	-1.805	361
0.8	511.2	-1.27	289.1
1.3	627.8	-0.6951	63.34
1.5	658	-0.5729	-42.74
1.9	448	-1.049	118.8

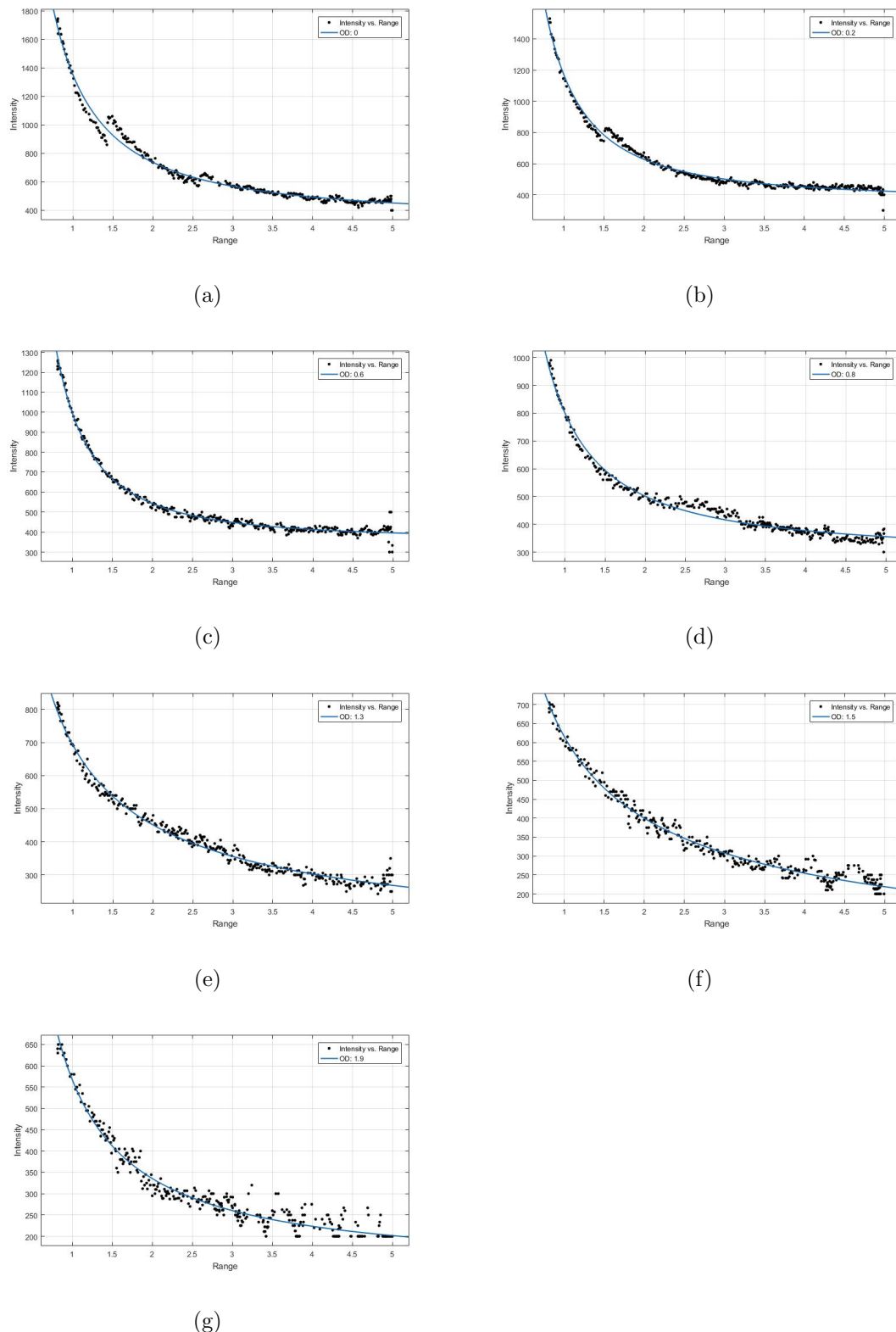


Figure 5.7: Curve fitting result of laser intensity vs. range in degraded environments

It can be observed that although the nominal intensity threshold of the LiDAR LS02A is 200. However, in the previous sets of data OD=0, 0.2, 0.6, 0.8, 1.3 (Figure 5.7 (a)(b)(c)(d)(e)), it is obvious that the maximum detection range is not only due to the intensity threshold. The resolution of position sensitive detector (PSD) is another reason, which makes the detection range reach the upper limit. From the principle of triangulation in Figure 2.1, we can see D cannot be infinite for the resolution of PSD, which is the minimum value of G . While the data of OD 1.5 and 1.9 (Figure 5.7 (f)(g)), the maximum LiDAR detection range is due to the intensity minimum threshold. Therefore, from the experimental results of the laser intensity vs. range, the maximum detection range of LiDAR may be composed of two aspects: first, the resolution of PSD; second, the laser intensity threshold of PSD. In addition, it can be observed from Figure 5.7 that intensity at 300 is a good value, which means I^* is set as 300. It is bigger than the nominal threshold, and it avoids unnecessary decrease of detection distance caused by too large value setting.

Laser point number vs. detection range

For LS02A, the detection angle is 86° and the angle resolution is $1^\circ/\text{laser point}$. In order to ensure the consistency of detection, in the experiment, only the middle 20 degrees are considered. This means that 20 laser points return in one scanning with 1 point representing 1° field angle. Under different experimental ambient conditions, laser return point number PN performs differently. Figure 5.8 shows the experimental results of laser point number vs. range. From the results, because the first four ambient conditions are relatively “good”, the data perform in a similar way that the laser point number of the detection is not lost until the maximum detection range, and always remains at 20 points. However, in a “bad” environment the last three sets of data, the laser point number attenuates seriously, so the analytic expressions for PN are set as piece-wise functions. And the larger the OD value is, which means the worse the environment is, the more serious the attenuation is. Table 5.2 is the

analytic expressions of laser point number vs. range in different environments.

In this study, the LiDAR detection performance is required to be a “conservative” style, so it is expected all laser point should be returned in the optimal case, which means PN^* is set as 20.

Table 5.2: Analytic expressions of laser point number vs. detection range

OD	$PN(R)$
0	$20(R \leq 4.5)$
0.2	$20(R \leq 4.5)$
0.6	$20(R \leq 4.5)$
0.8	$20(R \leq 4.5)$
1.3	$20(R \leq 3)$ $-4.791R^2 + 33.04 R - 37.5(R > 3)$
1.5	$20(R \leq 2.7)$ $-5.645 R + 34.21(R > 2.7)$
1.9	$20(R \leq 2)$ $-5.296 R + 28.14(R > 2)$

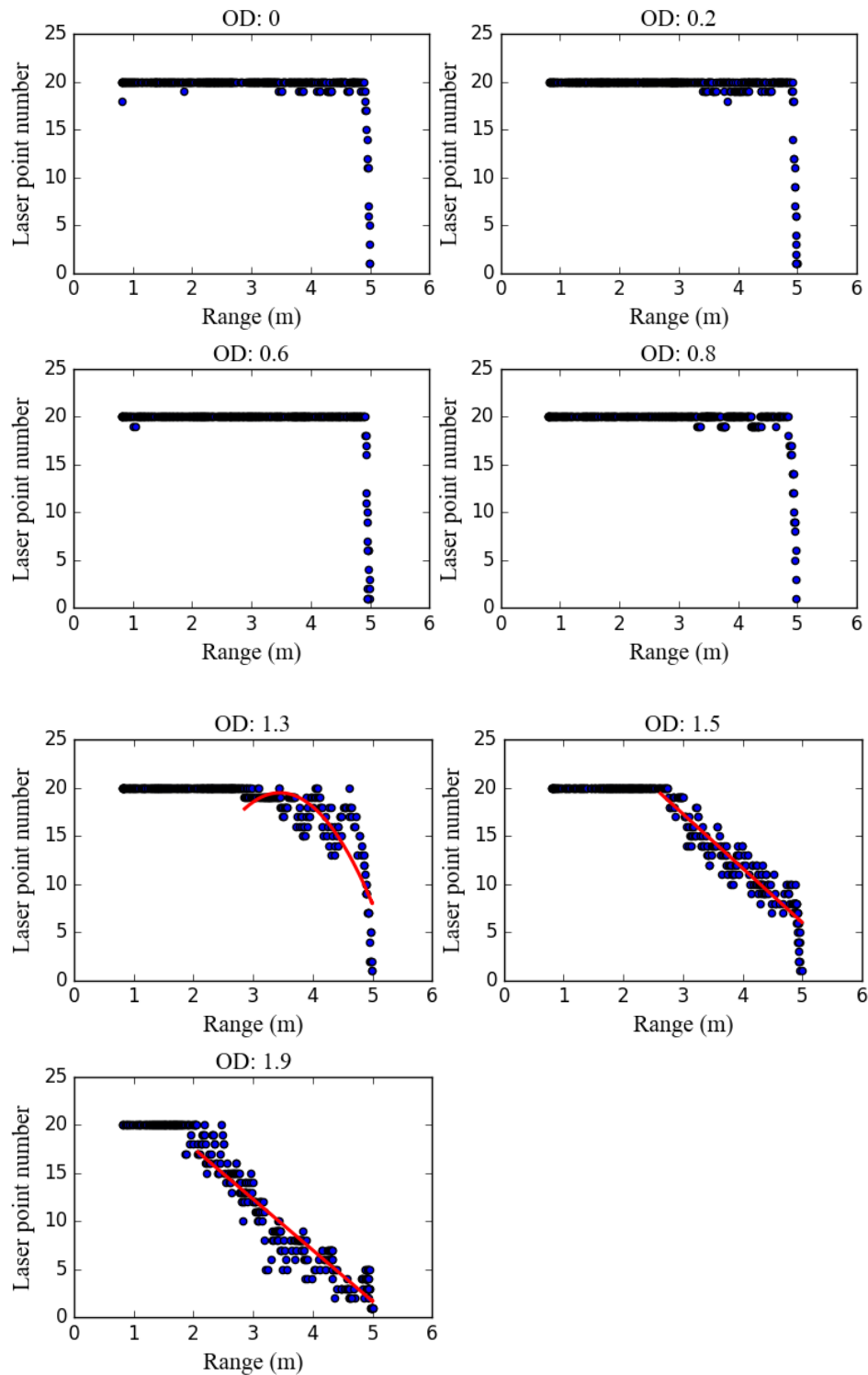


Figure 5.8: Experimental results and curve fitting of laser point number vs. range

Field of view vs. detection range

Based on Equation 4.1, $FOV(R)$ can be derived from $I(R)$ and $PN(R)$. The analytic expressions of FOV vs. detection range is detailed in Table 5.3

Table 5.3: Analytic expressions of laser point number vs. detection range

OD	$PN(R)$
0	$0.174R^2(R \leq 4.5)$
0.2	$0.174R^2(R \leq 4.5)$
0.6	$0.174R^2(R \leq 4.5)$
0.8	$0.174R^2(R \leq 4.5)$
1.3	$0.174R^2(R \leq 3)$ $-0.042R^4 + 0.29R^3 - 0.33R^2(R > 3)$
1.5	$0.174R^2(R \leq 2.7)$ $-0.049R^3 + 0.3R^2(R > 2.7)$
1.9	$0.174R^2(R \leq 2)$ $-0.046R^3 + 0.25R^2(R > 2)$

Thus, all $J(R)s$ in different ambient environments are obtained. From the previous data fitting and analytic expressions, a NN classification should be design to suitable for the available experimental platform. Four-class classification is a good choice because it is noted from the previous results that the results of the two sets of OD values of the nearest neighbors are close. Then, OD0 and OD0.2 are classified as EI_1 , OD0.6 and OD0.8 are as EI_2 , OD1.3 and OD1.5 are as EI_3 , OD1.9 is as EI_4 . Based on the knowledge of Section 2.2, a NN classification based on this experimental platform design can be derived. The scheme is like Figure 5.9. Note that each EI_n corresponds to two combination of ND filters as the difference exhibited by two combination is negligible.

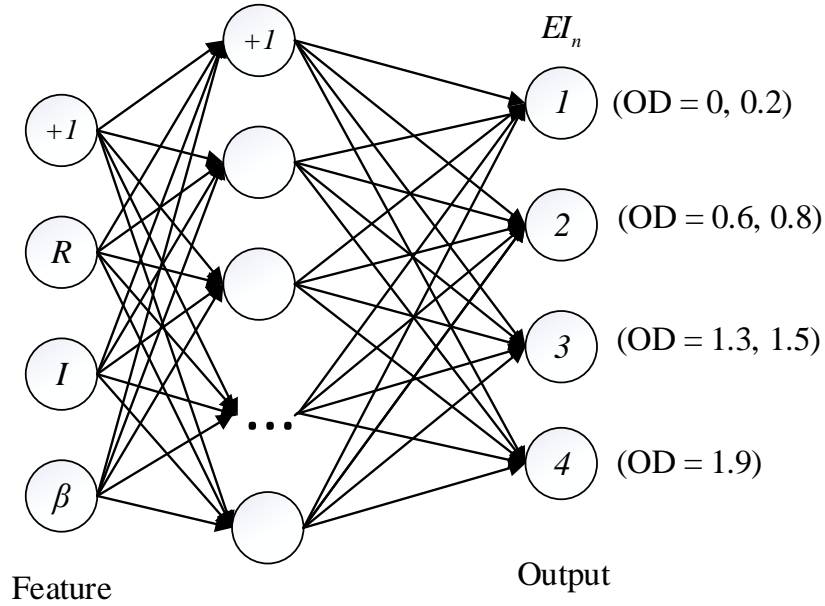


Figure 5.9: Neural network scheme of designed experimental platform

Combine the three performances, we can get the total cost function based on above three arguments. By tuning the minimum value of cost function (3.2) in a reasonable range. The parameters of the cost function (3.2) are $\alpha_1 = 0.5$, $\alpha_2 = 0.4$, $\eta_1 = 0.1$, $\eta_2 = 1$, and $\eta_3 = 10$. Therefore, the cost function used in off-line model-based optimization is

$$\begin{aligned} J(R) &= 0.5 \cdot 0.1 \cdot (I(R) - 300)^2 + 0.4 \cdot (PN(R) - 20)^2 - 0.1 \cdot 10 \cdot FOV(R) \\ &= 0.05 \cdot (I(R) - 300)^2 + 0.4 \cdot (PN(R) - 20)^2 - FOV(R) \end{aligned} \quad (5.1)$$

To sum up, the \widehat{R}^* in different ambient environments as indicated with EI_n can be obtained by solving an off-line optimization of the cost function (3.2), as shown in Table 5.4.

In addition,

Table 5.4: Off-line model-based optimal detection ranges \widehat{R}^*

EI_n	OD	Off-line model-based optimal detection ranges	
1	0	5	5
	0.2	5	
2	0.6	3.78	3.34
	0.8	3.34	
3	1.3	2.72	2.1
	1.5	2.1	
4	1.9	1.56	1.56

5.3 Experimental Results

A series of indoor experiments are executed to validate the characteristic and effectiveness of the model-guided ESC. The experiments consists of two parts: 1) experiment I: static detection optimization by model-guided esc for different targets in all experimental ambient conditions, at the same time a set of comparative experiments with only esc controller did to compare the experimental results; 2) experiment II: dynamic detection optimization to further validate the system's performance in more complicated ambient conditions.

In the following experimental plotting, all light blue curves * is LiDAR real-time detection range R from LiDAR point cloud, deep blue curves + is R_{ref} , orange triangle scatter Δ represents the real-time cost values and the upper colour bar in the pictures represents the EI . In detail, black represents EI_1 , yellow represents EI_2 , green represents EI_3 , and red represents EI_4 .

5.3.1 Experiment I

The detection targets in Experiment I is still and unchanged. The mobile carrier moves in one dimension and the direction is the normal of the detection target. The first two sets of the experiments shows the detection optimization of model-guided ESC in all experimental ambient conditions for two detection targets: wooden door and white paper, which shown in Figure 5.11. In the preliminary experiments, all detection target is a wooden door shown in Figure 5.10(a). This means in the model-based off-line optimization block in the system 4.1, the model mismatch is smallest for target (a) because the experimental conditions are closest to all off-line preliminary experiments.



Figure 5.10: Targets in Experiments I

Figure 5.11 shows the experiment results for target (a). When EI value increases, the stable optimal detection range decreases because in order to make up for the environmental degradation, a nearer detection range optimized to maintain the detection performance. The optimal detection range in EI_1 cases are around system boundary, the protection limit of the system affect the convergence of the range. However, because the costs are small enough, the dither signal still decayed and maintained in the minimum perturbation. Meanwhile, as an on-line optimization, the variation of

the other conditions are very small, which validate the benefit of the ESC with an attenuation dither signal.

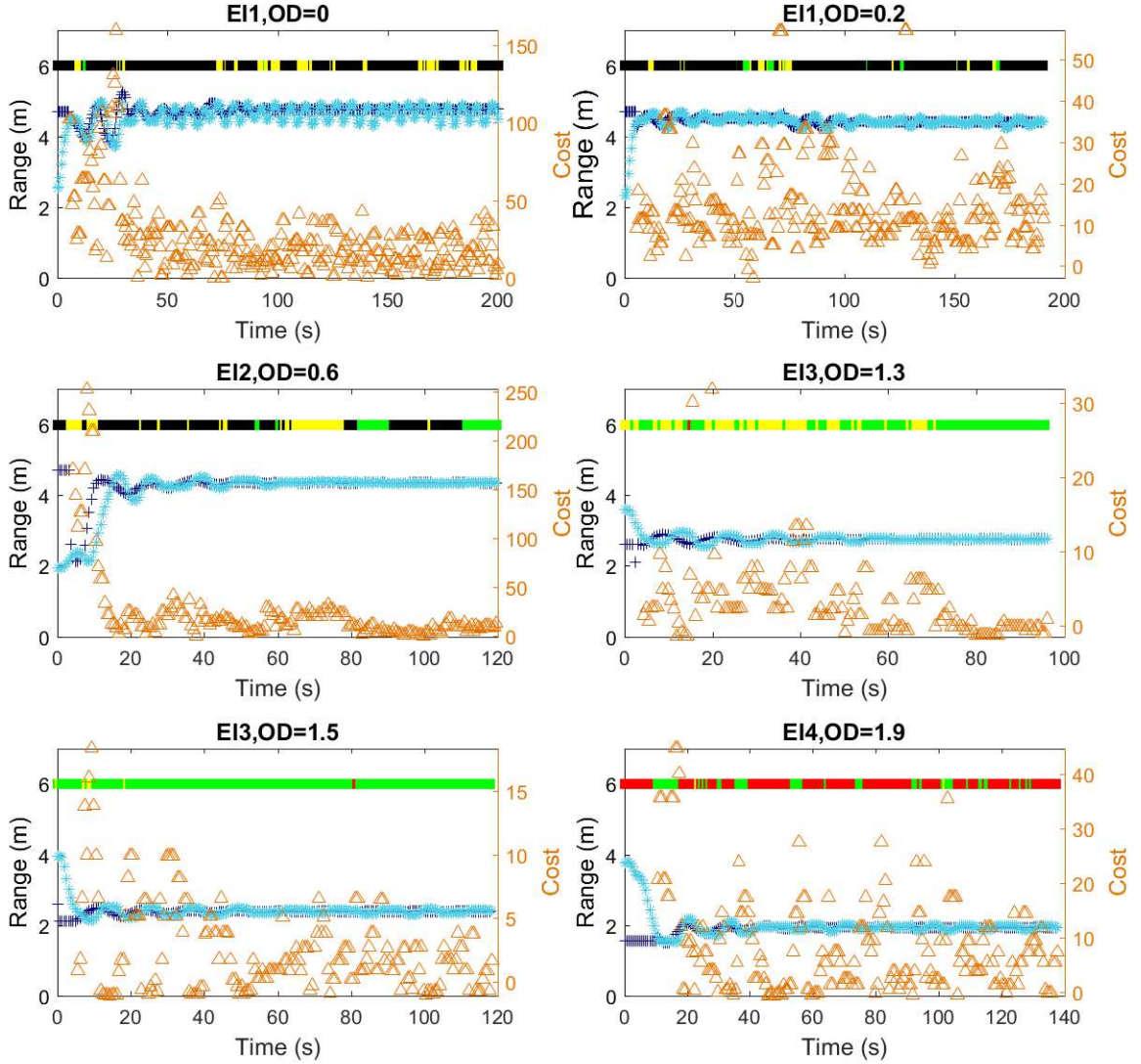


Figure 5.11: LiDAR static detection results under all EIs

The experiment in the case of EI_2 is described separately in detail. In Figure 5.12, the case of EI_2 dominates under the combination $OD=0.8$ of filters. It can be seen that the EI value jumps between EI_2 and EI_3 . In the first 75s of the process, many costs that not small enough, even some abnormal costs, makes the system reset the perturbation amplitude. So, the fluctuation of R_{ref} around 75s corresponds to

the resetting of dither signal amplitude in the ESC algorithm. This reset pushes the cost values to a lower level. These abnormal costs may arise from environmental disturbance or sensor disturbance.

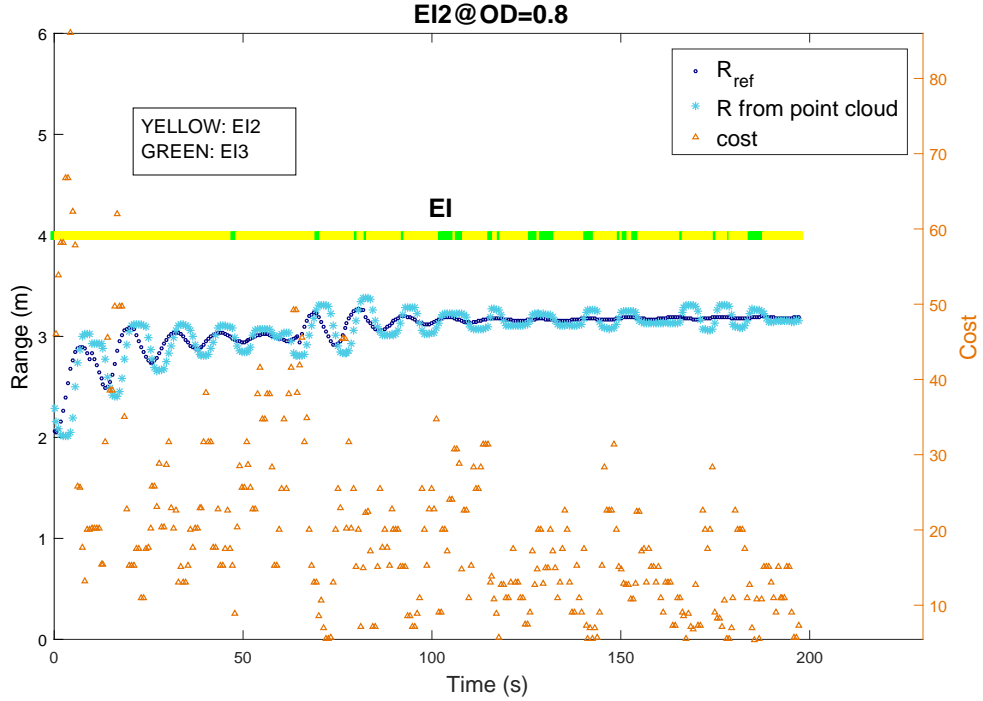


Figure 5.12: LiDAR static detection result under EI_2

The second experiment is executed as same experimental process of the first one, but different detection target. This time the target is set as white paper shown in Figure 5.10(b) and the detection results are shown in Figure 5.13. The trend of the experimental results is the same as previous ones in these same experimental environments. However, the detail of the three targeted performances and the final average optimal detection ranges

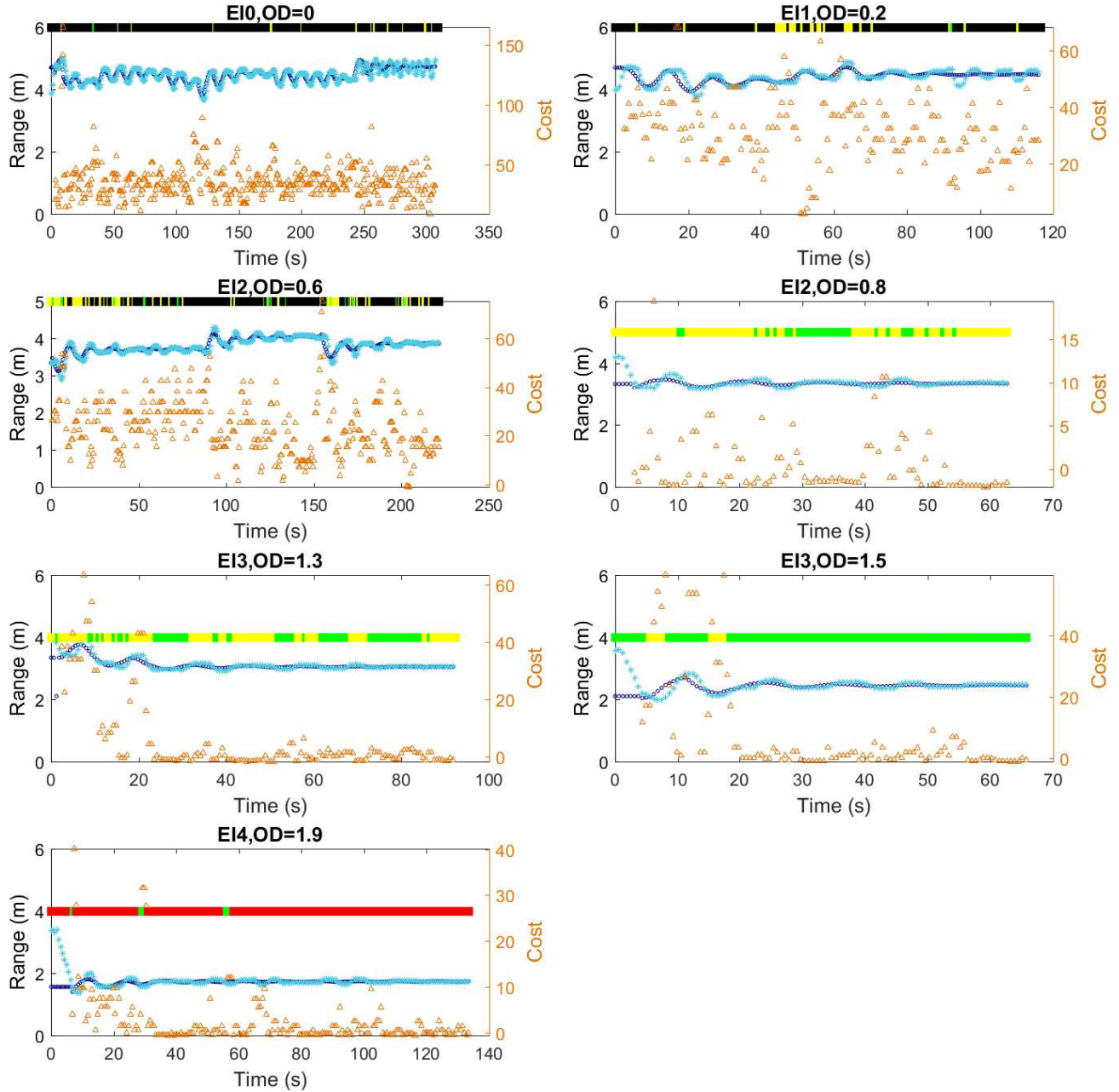


Figure 5.13: LiDAR static detection for white paper

The third group did the comparing experiments for the traditional perturbation-based ESC, and Figure 5.14 presents the results. As a comparative experiment, the experimental situation is simplified into 4 conditions. It is obvious that the results

of the model-guided ESC in Figure 5.11 are much better than the traditional ones in Figure 5.14: first, the convergent speed is fast. In Figure 5.14, the system converges to the neighborhood of the optima around 50s. While for the model-guided ESC, in most cases, the system can converge into a stable state in 20s. Even if in EI1,OD0, after entering ESC, there is still a period of optimization time due to the cost jitters, but it entered stable convergence in 40s; besides, the transient fluctuation in Figure 5.12 and 5.11 are much reduced in comparison with that in 5.14. Furthermore, the experiment analysis of model-guided ESC and the normal ESC about system settling time in 10% of final state and average cost is shown in Table 5.5 and Table 5.6. From the results, it is obvious that the most powerful strength of model-guided ESC compared to normal ESC is the settling time is much more fast. Because in model-guided ESC, the model-based part helps the system optimize the initial point of the ESC.

Table 5.5: Settling time (10% of final state) of model-guided ESC and traditional perturbation ESC

OD	0	0.6	1.3	1.9
Model-guided	27	14	4	17
ESC-only	63	175	40	35

Table 5.6: Average cost of model-guided ESC and traditional perturbation ESC in final state

OD	0	0.6	1.3	1.9
Model-guided	16.4	10.6	0.9	7.3
ESC-only	17.6	3.2	40.8	11.2

Table 5.7: Average laser intensity of model-guided ESC and traditional perturbation ESC in final state

OD	0	0.6	1.3	1.9
Model-guided	460	449	420	428
ESC-only	476	433	404	407

Table 5.8: Average laser point number of model-guided ESC and traditional perturbation ESC in final state

OD	0	0.6	1.3	1.9
Model-guided	18	19.1	20	20
ESC-only	19	19.4	19.1	19.9

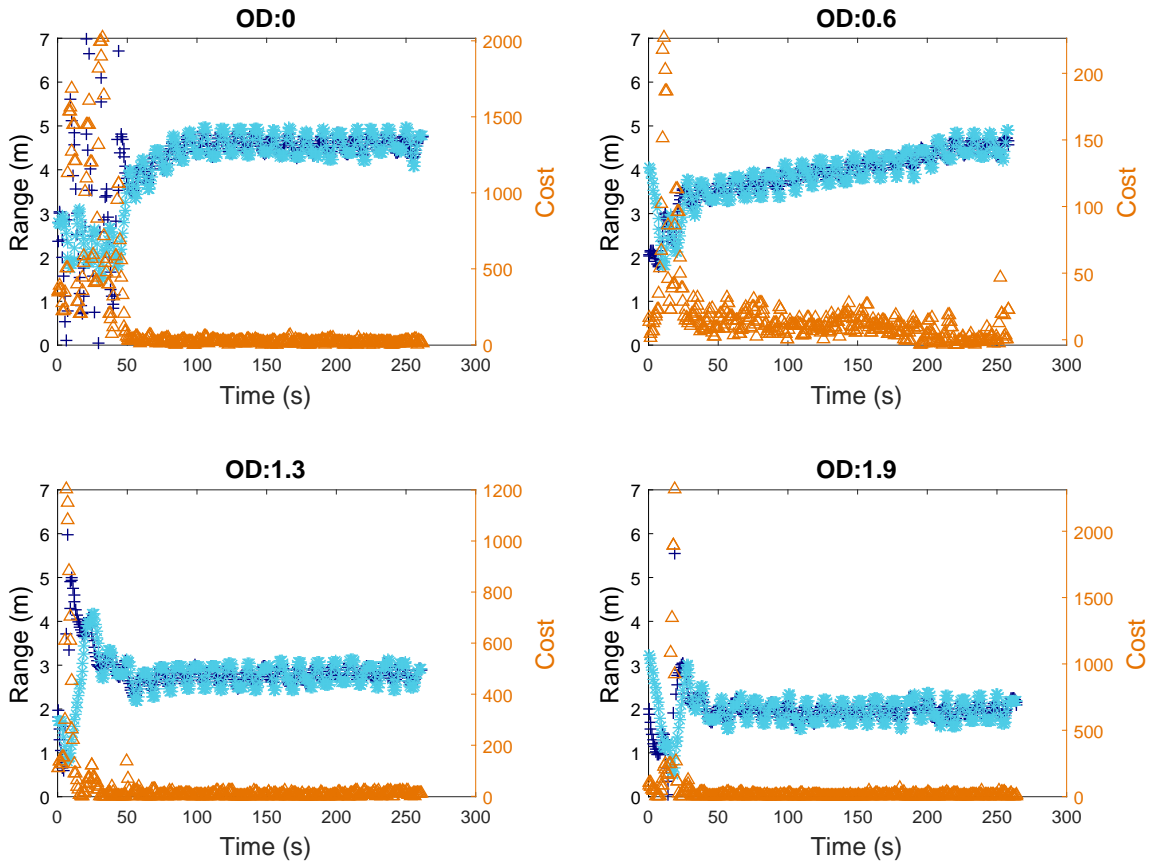


Figure 5.14: LiDAR detection results under all *EIs*

Table 5.9: Average FOV of model-guided ESC and traditional perturbation ESC in final state

OD	0	0.6	1.3	1.9
Model-guided(m^2)	3.4	3.1	1.3	0.6
ESC-only(m^2)	3.5	3.3	1.2	0.6

5.3.2 Experiment II

A group of dynamic experiments are executed to validate the dynamic performance of the model-guided ESC. Compared to experiment I, experiment II add a y-axis velocity to the mobile carrier. Figure 5.15 shows the targets in the dynamic detection, where are in the first floor of E.D. Lumley Centre for Engineering Innovation (CEI) in University of Windsor. During the entire detection process, targets consists of 4 parts: white wall, matte silver metal (the garbage bin), smooth silver metal (bottom of the door) and surface mixed with wooden board and white wall. (The height of the mobile carrier is just at the junction of the wooden board and the white wall. Considering the divergence of the emitted laser, the LiDAR may detect two materials at the same time.). The mobile carrier starts from the position of the starting line, and the distance between the starting position and the wall is arbitrary to prove that the subsequent optimization process is not affected by the initial start position.

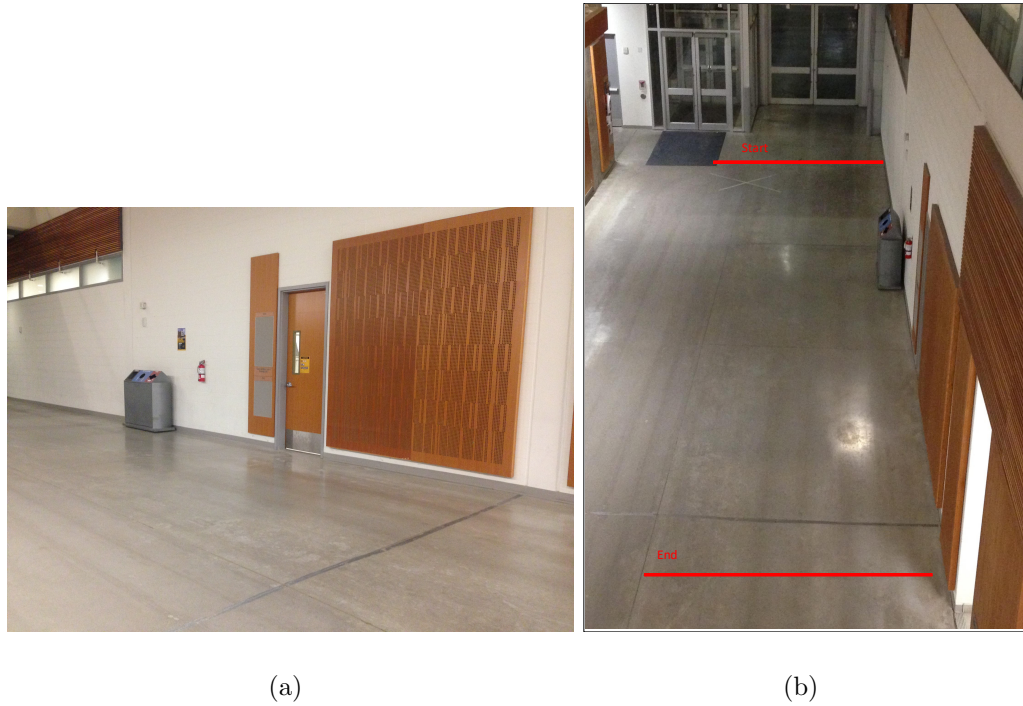


Figure 5.15: Targets in dynamic detection

Figure 5.16 shows the dynamic performance of the model-guided ESC. In the dynamic detection algorithm, when $J > J_{abn}$, the movement of mobile carrier in y axis pauses in order to give the ESC enough time to search the new operating point and this process maybe a long time because of ESC's nature. Due to this reason, the performances for the dynamic detection is poor and different in various conditions. The main two disturbance of the entire detection is the garbage bin and the smooth silver mental of bottom of the door in Figure 5.15. In the results, the LiDAR detected the garbage bin in 40s to 50s according to different cases, which is the first disturbance of the entire process. However, the performances are very different in different cases, in OD=0, 0.2 and 0.9 the first disturbance had a noticeable effect on the detection process, especially in OD=1.9 the mobile carrier oscillate much time to search for working point that meets the conditions of the algorithm. The second main disturbance is the smooth silver mental, the detection performances also performed

in different ways. OD=0, 0.6 and 1.3 had little responses to this disturbance.

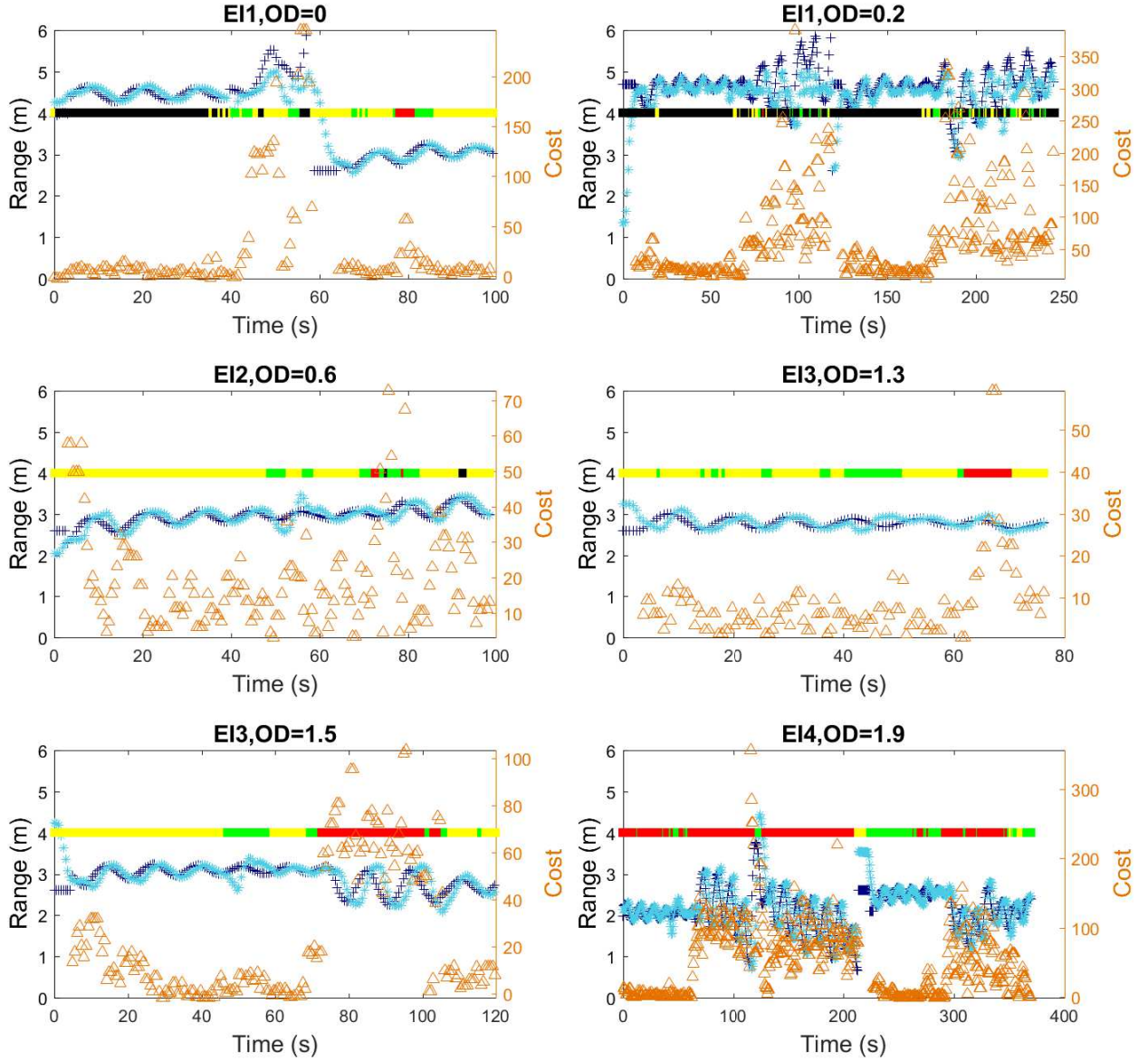


Figure 5.16: Targets in dynamic detection

At the same time, the system has some common characteristics for all cases. When the detection target changed, EI changed accordingly in most cases. Furthermore, the model-guided ESC succeeds in reducing the cost value J , which represents a higher detection performance, unless the cost value was already small like OD=0,

1.3. However in other cases, the optimization is obvious.

Some experimental videos are shown in YouTube: <https://youtu.be/GkF78Vwy0To>.

5.4 Conclusion

From the previous experiments, the model-guided ESC is proved to be effective, also the system can be summarized with several characteristics. First, when atmospheric attenuation is larger, the average cost value is smaller because the intensity part in cost function (3.2) becomes smaller. This means that once the LiDAR worked in a relatively “good” environment encounters disturbances, it will take a long time to search the operating point, furthermore it would be longer due to the dither of the ESC.

Second, by comparing the traditional ESC and model-guided ESC, the model-guided method helps the system reach the operating point faster with the off-line optimization. However, this method is not perfect, once the prediction of EI deviates greatly from the actual one, the system will take longer time to optimize. Moreover, EI based on learning algorithm needs further development. Third, the previous results prove the necessity of using ESC to compensate the model mismatch. In static detection, when the optimization is completed, there is a certain stability error with the value in Table 5.4. At the same time, although the detection target is different with training process in preliminary experiment, the model-based ESC worked well, which means the system has strong robustness because ESC has high robustness.

Chapter 6

Conclusion

In this paper a model-guided ESC structure is proposed to regulate the LiDAR detection range optimally and automatically in order to guarantee satisfied LiDAR detection performance under varying ambient environments. An environmental index EI is designed to classify the ambient environment conditions, and data-induced analytic models are synthesized for the relation between the LiDAR performance and detection range. Essentially, a model-based off-line optimization is combined with an on-line ESC algorithm to deliver the scheme of the desired mechanism. The experimental results are presented to validate the effectiveness of the proposed model-guided ESC structure which is shown to perform better than the traditional perturbation-based ESC only in terms of the convergent rate.

6.1 Summary of Contribution

The contributions of this study are twofold:

First, an Environment Index (EI) is proposed based on a trained neural network model for the relation between LiDAR point cloud data and the ambient condition, which is used to (approximately) classify the impact of different ambient condition on LiDAR performance. Besides, this EI is also used as part of the switching criterion

to re-initialize the ESC algorithm for different ambient conditions.

Second, a model-guided ESC is proposed to optimize the LiDAR detection range, which consists of an ESC algorithm, a class of off-line optimized LiDAR detection range values based on a customized cost function for different ambient condition, and a switching mechanism, all indexed by the EI . The proposed optimization structure improves the convergence performance of the ESC algorithm while making up the deficiency of integrity due to modeling inaccuracy in the off-line optimization solutions.

6.2 Future Work

In this thesis, the cost function for ESC and off-line optimization are customized, which based on author's own consideration. However, in real projects, the task of the project and objectives of the mission decide the cost function. In future work, a task model should be considered to match the model-guided ESC system. Besides, in this research, the application of neural networks is very important as a means of obtaining EI . However, this paper does not focus on the optimization and design of neural network, with the development of deep learning, the better neural network structure design can help prediction of EI more accurate. Also, the classification of EI and the according off-line models could be fine to improve the whole system.

Appendix A

The specification of LS02A is shown as follow, which provided by LeiShen Intelligent System Company.

Item	Unit	Min	Default	Max	Note
Laser wavelength	(nm)	788	792	794	infrared band (25°C)
Laser power	(mW)		0.3		Average power
Detection range	(m)		0.1~4		Reflectivity under 70%
Detection Accuracy	(mm)		<2%	of distance	
Detection Angle	(Deg)		86		
Angle resolution	(Deg)		1		customized
Scan frequency	(Hz)		10		
Volume	(mm ³)		65×40×40		
Weight	(g)		50		

Appendix B

Parameters in neural network model is shown in this section. The data scaling, training, encapsulation and use of the neural network is based on Scikit-learn. Moreover, most algorithm of this thesis please refer author's Github:

https://github.com/YouyingHua/Master_Project.

Scaling of features of LiDAR data:

```
sklearn.preprocessing.StandardScaler(copy=True, with_mean=True, with_std=True)
```

Model description and technical details of Neural network:

```
MLPClassifier(activation='relu', alpha=0.0001, batch_size='auto', beta_1=0.9, beta_2=0.999,  
early_stopping=False, epsilon=1e-08, hidden_layer_sizes=(100,), learning_rate='constant',  
learning_rate_init=0.001, max_iter=200, momentum=0.9, nesterovs_momentum=True,  
power_t=0.5, random_state=None, shuffle=True, solver='adam', tol=0.0001, validation_fraction=0.1,  
verbose=False, warm_start=False)
```

Size of the neural network: [(4, 100), (100, 4)]

Layer number of the neural network: 3

Bibliography

- [1] R. Merriam, R. Merriam, Ruddy, Crenn, E. Johansson, Bill, J. Homer, David, John, D. Schegh, and et al., “Principle of triangulation.” <https://hackaday.com/2016/01/22/how-to-use-lidar-with-the-raspberry-pi/>, Jan 2016.
- [2] J. Wojtanowski, M. Zygmunt, M. Kaszczuk, Z. Mierczyk, and M. Muzal, “Comparison of 905 nm and 1550 nm semiconductor laser rangefinders’ performance deterioration due to adverse environmental conditions,” *Opto-Electronics Review*, vol. 22, pp. 183–190, Sep 2014.
- [3] S. Michaud, “Influence of complex environments on lidar-based robot navigation,” 2016.
- [4] M. Sanfourche, J. Delaune, G. Le Besnerais, H. De Plinval, J. Israel, P. Cornic, A. Treil, Y. Watanabe, and A. Plyer, “Perception for UAV: Vision-Based Navigation and Environment Modeling.,” *AerospaceLab*, pp. p. 1–19, May 2012.
- [5] Y. Tan, W. H. Moase, C. Manzie, D. Nešić, and I. M. Y. Mareels, “Extremum seeking from 1922 to 2010,” *Proceedings of the 29th Chinese Control Conference*, pp. 14–26, 2010.
- [6] J. Ebegbulem and M. Guay, “Distributed extremum seeking control for wind farm power maximization,” *IFAC-PapersOnLine*, vol. 50, no. 1, pp. 147 – 152, 2017. 20th IFAC World Congress.

- [7] D. Krishnamoorthy, J. Ryu, and S. Skogestad, “A dynamic extremum seeking scheme applied to gas lift optimization,” *IFAC-PapersOnLine*, vol. 52, no. 1, pp. 802 – 807, 2019. 12th IFAC Symposium on Dynamics and Control of Process Systems, including Biosystems DYCOPS 2019.
- [8] Q. Tan, P. Divekar, Y. Tan, X. Chen, and M. Zheng, “A diesel engine combustion phasing optimization using a model guided extremum seeking approach,” in *2016 35th Chinese Control Conference (CCC)*, pp. 2837–2842, July 2016.
- [9] Z. Cao, E. Dassau, R. Gondhalekar, and F. J. Doyle III, “Extremum seeking control based zone adaptation for zone model predictive control in type 1 diabetes,” *IFAC-PapersOnLine*, vol. 50, no. 1, pp. 15074–15079, 2017.
- [10] C. Goodin, D. Carruth, M. Doude, and C. Hudson, “Predicting the influence of rain on lidar in adas,” *Electronics*, vol. 8, no. 1, 2019.
- [11] R. H. Rasshofer, M. Spies, and H. Spies, “Influences of weather phenomena on automotive laser radar systems,” *Advances in Radio Science*, vol. 9, pp. 49–60, 2011.
- [12] D. Atlas, “Optical extinction by rainfall,” *Journal of Meteorology*, vol. 10, no. 6, pp. 486–488, 1953.
- [13] M. Grabner and V. Kvicera, “Comparison of extinction in fog and rain on terrestrial propagation paths,” in *2011 Loughborough Antennas & Propagation Conference*, pp. 1–4, IEEE, 2011.
- [14] M. A. A. Ali and M. A. Mohammed, “Effect of atmospheric attenuation on laser communications for visible and infrared wavelengths,” *Journal of Al-Nahrain University-Science*, vol. 16, no. 3, pp. 133–140, 2013.

- [15] I. Ashraf and Y. Park, "Effects of fog attenuation on lidar data in urban environment," in *Smart Photonic and Optoelectronic Integrated Circuits XX*, vol. 10536, p. 1053623, International Society for Optics and Photonics, 2018.
- [16] J. Guo and X.-J. Zhao, "Attenuation characterization of 532 nm and 1064 nm laser propagating in rain," *Optik*, vol. 127, no. 20, pp. 9088–9094, 2016.
- [17] S. T. Shipley, E. Eloranta, and J. Weinman, "Measurement of rainfall rates by lidar," *Journal of Applied Meteorology*, vol. 13, no. 7, pp. 800–807, 1974.
- [18] I. I. Kim, B. McArthur, and E. J. Korevaar, "Comparison of laser beam propagation at 785 nm and 1550 nm in fog and haze for optical wireless communications," in *Optical Wireless Communications III*, vol. 4214, pp. 26–37, International Society for Optics and Photonics, 2001.
- [19] S. Shah, S. Mughal, and S. Memon, "Theoretical and empirical based extinction coefficients for fog attenuation in terms of visibility at 850 nm," in *2015 International Conference on Emerging Technologies (ICET)*, pp. 1–4, IEEE, 2015.
- [20] J. Guo, H. Zhang, and X.-j. Zhang, "Propagating characteristics of pulsed laser in rain," *International Journal of Antennas and Propagation*, vol. 2015, 2015.
- [21] A. Filgueira, H. González-Jorge, S. Lagüela, L. Díaz-Vilariño, and P. Arias, "Quantifying the influence of rain in lidar performance," *Measurement*, vol. 95, pp. 143–148, 2017.
- [22] M. Kutila, P. Pyykönen, W. Ritter, O. Sawade, and B. Schäufele, "Automotive lidar sensor development scenarios for harsh weather conditions," in *2016 IEEE 19th International Conference on Intelligent Transportation Systems (ITSC)*, pp. 265–270, IEEE, 2016.

- [23] R. Nebuloni, "Empirical relationships between extinction coefficient and visibility in fog," *Applied optics*, vol. 44, no. 18, pp. 3795–3804, 2005.
- [24] R. Heinzler, P. Schindler, J. Seekircher, W. Ritter, and W. Stork, "Weather influence and classification with automotive lidar sensors," in *2019 IEEE Intelligent Vehicles Symposium (IV), Paris, F, June 9-12, 2019*, pp. 1527–1534, IEEE, Piscataway, NJ, 2019.
- [25] M. Krstić and H.-H. Wang, "Stability of extremum seeking feedback for general nonlinear dynamic systems," *Automatica*, vol. 36, no. 4, pp. 595 – 601, 2000.
- [26] D. Krishnamoorthy, A. Pavlov, and Q. Li, "Robust extremum seeking control with application to gas lifted oil wells," *IFAC-PapersOnLine*, vol. 49, no. 13, pp. 205 – 210, 2016. 12th IFAC Workshop on Adaptation and Learning in Control and Signal Processing ALCOSP 2016.
- [27] Z. Cao, E. Dassau, R. Gondhalekar, and F. J. D. III, "Extremum seeking control based zone adaptation for zone model predictive control in type 1 diabetes
**this work is supported by the national institutes of health grants dp3dk094331, dp3dk104057 and uc4dk108483.," *IFAC-PapersOnLine*, vol. 50, no. 1, pp. 15074 – 15079, 2017. 20th IFAC World Congress.
- [28] C. Dehong, Z. Liangqi, S. Pengpeng, T. Zaiyang, M. Yuhao, and W. Yong, "Design and implementation of lidar navigation system based on triangulation measurement," in *2017 29th Chinese Control And Decision Conference (CCDC)*, pp. 6060–6063, IEEE, 2017.
- [29] P. Church, "3d lidar imaging in obscurants," 2014.
- [30] C. Bohren and D. Huffman, "Absorption and scattering of light by small particles," *CF Bohren, & DR Huffman*, 1983.

- [31] “Study of laser propagation and attenuation through the rain and fog environment,” Master’s thesis, Xi’an University of Technology.
- [32] K. M. Czajkowski and M. Schmid, “Durable and cost-effective neutral density filters utilizing multiple reflections in glass slide stacks,” *IEEE Photonics Journal*, vol. 9, no. 6, pp. 1–11, 2017.
- [33] Z. Zhang, T. R. Gentile, A. L. Migdall, and R. Datla, “Transmittance measurements for filters of optical density between one and ten,” *Applied optics*, vol. 36, no. 34, pp. 8889–8895, 1997.
- [34] C. Nicholson, “Multilayer perceptrons (mlp).” <https://skymind.ai/wiki/multilayer-perceptron#mlp>. A Beginner’s Guide to Multilayer Perceptrons (MLP).
- [35] “Neural network models (supervised).” https://scikit-learn.org/stable/modules/neural_networks_supervised.html.
- [36] I. Goodfellow, Y. Bengio, and A. Courville, *Deep learning*. MIT press, 2016.
- [37] “Softmax function.” https://en.wikipedia.org/wiki/Softmax_function. Softmax function.
- [38] J. Hale, “Standardscaler in scikit-learn.” <https://towardsdatascience.com/scale-standardize-or-normalize-with-scikit-learn-6ccc7d176a02>. Scale, Standardize, or Normalize with Scikit-Learn.
- [39] S. Wang, “Phase-based extremum seeking control,” 2016.
- [40] M. Krstic, “Extremum seeking control,” *Encyclopedia of Systems and Control*, pp. 413–417, 2015.
- [41] Y. Tan, D. Nešić, and I. Mareels, “On non-local stability properties of extremum seeking control,” *Automatica*, vol. 42, no. 6, pp. 889–903, 2006.

- [42] J. Tang, “Distributed formation control for ground vehicles with visual sensing constraint,” Master’s thesis, University of Windsor, Windsor, Ontario, Canada, 2019.
- [43] M. Quigley, B. Gerkey, and W. D. Smart, *Programming Robots with ROS: a practical introduction to the Robot Operating System.* ” O’Reilly Media, Inc.”, 2015.
- [44] “scikit-learn.” <https://en.wikipedia.org/wiki/Scikit-learn>. A free software machine learning library for the Python programming language.

Vita Auctoris

Name: Youying Hua

Place of Birth: Shanghai, China

Year of Birth: 1990

Education: High School (Shanghai No.54 High School, Shanghai)
2005-2008

Bachelor's Degree (Shanghai University of Engineering Science, Shanghai)
2008-2012

Master's Degree (University of Windsor, Windsor)
2016-2019

Work Experience: Shanghai Cigarette Factory
2012-2016